Solar Phys (2020) 295:61
https://doi.org/10.1007/s11207-020-01624-0

INVITED REVIEW & EDITOR'S CHOICE

ICME Evolution in the Inner Heliosphere

J.G. Luhmann[1] · **N. Gopalswamy**[2] · **L.K. Jian**[2] · **N. Lugaz**[3]

Received: 3 September 2019 / Accepted: 3 April 2020 / Published online: 23 April 2020

Abstract ICMEs (interplanetary coronal mass ejections), the heliospheric counterparts of what is observed with coronagraphs at the Sun as CMEs, have been the subject of intense interest since their close association with geomagnetic storms was established in the 1980s. These major interplanetary plasma and magnetic field transients, often preceded and accompanied by solar energetic particles (SEPs), interact with planetary magnetospheres, ionospheres, and upper atmospheres in now fairly well-understood ways, although their details and context affect their overall impacts. The term ICME as it is used here refers to the complete solar-wind plasma and field disturbance, including the leading shock (if present), the compressed, deflected solar-wind plasma and the field behind the shock ("sheath"), and the coronal ejecta (the "driver") – often called a magnetic cloud. Many uncertainties remain in understanding both the relationship to what is observed at the Sun and the variety of local outcomes suggested by *in-situ* observations. This impacts our abilities to interpret events and to forecast effects based on solar observations. Here, we briefly consider what is known about ICMEs and their evolution *en route* from the Sun from the combination of available observations and interpretive models that have been developed up to now. The included references are only representative of the large body of work that has been published on this subject. Our aim is to provide the reader with an updated synthesis of research results in this still active area of heliophysics at the dawn of the *Parker Solar Probe* (PSP) and *Solar Orbiter* (SO) mission era.

Keywords ICME · CME · Space weather

✉ J.G. Luhmann
jgluhman@ssl.berkeley.edu

1 Space Sciences Laboratory, University of California, Berkeley, CA, USA

2 NASA Goddard Space Flight Center, Greenbelt, MD, USA

3 Space Science Center and Department of Physics, University of New Hampshire, Hanover, NH, USA

1. Introduction

Since their recognition as the primary causes of space weather storms (*e.g.* Wilson, 1987; Gosling, 1993; see Gopalswamy (2016) for a historical review), Coronal Mass Ejections (CMEs), and the Interplanetary Coronal Mass Ejection (ICME) disturbances that they produce in the solar wind, have been a focus of heliophysics research. Both the physical origins of CME events in the solar corona, and the resulting ICME plasma and field features in *in-situ* observations – here comprised of the leading shock and sheath compression together with the coronal material or "ejecta" – continue to be scientific targets of space mission investigations including the recently launched *Parker Solar Probe* (Fox *et al.*, 2016) and *Solar Orbiter* (Müller *et al.*, 2020). In addition, our understanding of the relationships of ICMEs to the CMEs observed by coronagraphs and extreme ultra-violet (EUV) imagers is particularly important because of its potential for forecasting the many local impacts of this form of solar activity (*e.g.* Russell, 2000; Borovsky and Denton, 2006; Burns *et al.*, 2007; Conner *et al.*, 2016; Reiff *et al.*, 2016). Progress has been significantly enhanced by the availability of multi-perspective imaging using combinations of *Solar and Heliospheric Observatory* (SOHO) and *Solar Terrestrial Relations Observatory* (STEREO) observations, starting in 2007. Those observations, together with STEREO/*Heliospheric Imager* (HI: Harrison *et al.*, 2018) white-light images that extended the field of view up to ≈ 1.5 AU, and spatially separated *in-situ* plasma and field measurements, reinforced the idea that the erupting structures seen in the corona become the drivers in their ICME counterparts. The results supported the results of earlier studies (*e.g.* starting with Burlaga *et al.*, 1981; Klein and Burlaga, 1982; Marubashi, 1986; Lepping, Burlaga, and Jones, 1990) that envisioned expanding flux ropes, still partially attached to the Sun at both ends, plowing outward through the ambient solar-wind plasma and magnetic field – sometimes forming a leading shock as illustrated in Figure 1. This basic picture of an ICME and its coronal connection has been applied for decades to *in-situ* plasma and field measurement interpretations, heliospheric models, and geomagnetic-storm predictions that depend on knowing the arriving ICME speed and whether the structure includes southward (-Bz) interplanetary magnetic field (*e.g.* Gonzalez and Tsurutani, 1987; Wilson, 1987; Russell, 2000). However, the multi-point perspectives and *in-situ* samplings tell us that the Sun-to-1 AU evolution is rarely the simple, self-similar flux-rope expansion picture suggested here.

Prediction of ICME properties at 1 AU from coronal observations of CMEs continues to be an elusive goal, as CMEs can deflect from a radial trajectory, can erode or merge with other structures, and can undergo non-uniform accelerations and decelerations in the course of their outward motion (see recent reviews by Manchester *et al.*, 2017; Kilpua, Koskinen, and Pulkkinen, 2017; Cremades, 2018). Simply connecting particular CMEs with the ICMEs that they produce is often difficult when the solar event signatures are not clearly observed or isolated from other activities. In addition, *in-situ* sampling is notoriously limited in its ability to provide a complete picture of an ICME's large-scale structure. These complications, coupled with uncertainties regarding the CME initiation process(es) in the corona (see review by Green *et al.*, 2018, for example) have made it difficult to apply the early picture to both retrospective interpretations of well-observed events and potential geomagnetic-storm forecasting schemes. Thus, part of the strategy in designing the PSP and SO missions has been the prospect of revealing more insight into both the coronal roots of ICMEs and the roles played by their context and interactions as they evolve from coronal to interplanetary structures near the PSP perihelion of ≈ 10 $R_{\odot}$.

This overview provides a brief picture of ICME radial evolution between the corona and 1 AU as it is seen today. In Section 2 we revisit what has been learned based in large part on

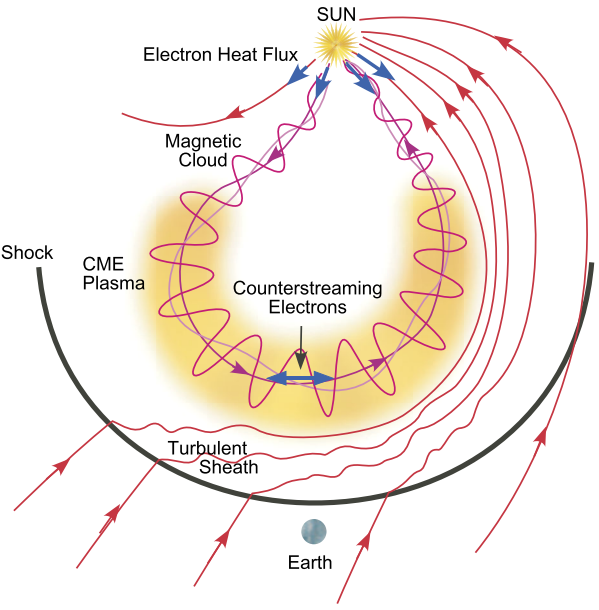

Figure 1 This "standard" picture of an ICME developed decades ago (*e.g.* Burlaga *et al.*, 1981; from Zurbuchen and Richardson, 2006) includes the basic features that we assume today: the leading shock, a compressed ambient solar-wind "sheath" where the magnetic field may be perturbed by the shock and foreshock, and a shock "driver" consisting of the coronal "ejecta" including a flux-rope-like magnetic-field structure. Although this picture remains widely used, it leaves out some important details that continue to challenge our understanding and applications of this concept. (Image reproduced with permission from Zurbuchen and Richardson (2006), copyright by Springer.)

solar and heliospheric imaging, in Section 3 we consider the additional information gleaned from radio emissions, in Section 4 we summarize some key results from *in-situ* plasma, magnetic field, and energetic particle measurements, and in Section 5 we consider how far modeling efforts have been able to capture the full range of the observed ICME generation and propagation phenomena. Finally in Section 6 some thoughts on anticipated future contributions are offered. We end with an updated illustration of how the original concept in Figure 1 has evolved as a result of improved observations and interpretive modeling, and still-open questions to be addressed with the new perspectives and capabilities of the *Parker Solar Probe* (PSP) and *Solar Orbiter* (SO).

2. ICME Radial Evolution: As Revealed Through Images

Attempts to deduce the three-dimensional (3D) structure of coronal eruptions based on their appearance in two-dimensional images have been made for a long time (*e.g.* see Rouillard, 2011; Webb and Howard, 2012, and the references therein). Although there are sometimes narrow, "jet"-like transients observed in the corona (*e.g.* Vourlidas *et al.*, 2017; Sterling, 2018), most CME "ejecta" near the Sun have been described as flux ropes (Mouschovias and Poland, 1978; Chen *et al.*, 1997), ice-cream cone shaped bundles of coronal plasma and field (Fisher and Munro, 1984), or spheromak-like flux toroids (*e.g.* Vandas *et al.*, 1997; Gopalswamy *et al.*, 2009a). Such models are still in vogue in various forms (*e.g.* Xie, Ofman, and Lawrence, 2004; Xie *et al.*, 2006; Shiota and Kataoka, 2016; Nieves-Chinchilla *et al.*, 2018, 2019). Multi-perspective coronal imaging is now routinely used to determine the CME-ejecta orientations and propagation directions while they are still in the corona, assuming a croissant-like shape with its ends on the Sun. One of the main techniques is the graduated cylindrical shell (GCS) model (Thernisien, Vourlidas, and Howard, 2009; Thernisien, 2011), although there exist several alternatives (*e.g.* Isavnin, 2016). Addition of a model for the initial ICME shock in the form of a spheroid surrounding the ejecta has made the picture

of what is observed more complete (Olmedo *et al.*, 2013; Hess and Zhang, 2014; Mäkelä *et al.*, 2015; Kwon, Zhang, and Vourlidas, 2015; Xie *et al.*, 2017; Kwon and Vourlidas, 2017). But how do these features evolve into their heliospheric counterparts? Are there features that are distinctly coronal phenomena? The coronal flux rope plus shock system is envisioned to undergo changes as it interacts with neighboring large-scale structures of coronal streamers and coronal holes (Gopalswamy *et al.*, 2009b; Wood *et al.*, 2012; Kay and Opher, 2015; Liewer *et al.*, 2015), current sheets (Yurchyshyn, Abramenko, and Tripathi, 2009; Isavnin, Vourlidas, and Kilpua, 2014), other CMEs and ICMEs (Gopalswamy *et al.*, 2001a; Lugaz *et al.*, 2017a), and in the ambient solar wind with its spiral-shaped interacting stream structures (Gopalswamy *et al.*, 2001b; Savani *et al.*, 2010; Vršnak *et al.*, 2013, 2014; Wang *et al.*, 2014). Work comparing the CME orientation in the corona to the ICME orientation at 1 AU often finds large deviations (Isavnin, Vourlidas, and Kilpua, 2013; Wood *et al.*, 2017; Palmerio *et al.*, 2018), although it is not clear if these are due to CME rotation or limitations of the fitting and reconstruction methods (*e.g.* Al-Haddad *et al.*, 2013). Clear CME rotation is seen in coronal images (*e.g.* Kay and Opher, 2015) but it is unclear how much more occurs in interplanetary space. In addition, different types of interactions dominate at different phases of the solar cycle (Gopalswamy, Tsurutani, and Yan, 2015): Inter-CME and inter-ICME interactions dominate in the maximum phase because of the high rate of CMEs. At solar quiet times, the eruptions may be channeled toward the Equator when large polar coronal holes are present, while in the declining phase they may interact more with equatorial and mid-latitude coronal holes and their solar-wind streams. The outcomes of these interactions also depend on the intrinsic CME properties. A wide, fast eruption may evolve quite self-similarly, relatively unaffected by its surroundings, while a weak or even moderate event readily merges with the ambient solar-wind stream structure.

One of the primary motivations for coronal and heliospheric imaging studies is to determine whether the ICME shock strength, speed, and Bz (or north–south) magnetic-field component measured at 1 AU can be inferred from the CME structure and speed in the corona. While density and speed determinations from images and sequences of images, respectively, are relatively straightforward, the magnetic field determination from images has continued to present challenges. Although the fundamental structure of CMEs typically involves a magnetic-flux rope, they generally expand, distort and deflect as they interact with their surroundings *en route* to 1 AU. Their ICME counterparts, best represented by the *in-situ* signatures called magnetic clouds (MCs), are characterized by strong magnetic fields, smooth field rotations over large angles, low accompanying ion temperatures, and low plasma β (*e.g.* Klein and Burlaga, 1982). Additionally, the handedness, or helicity, of the field in the active region from which a CME originates agrees with the apparent twist of the ICME ejecta fields for sometimes large fractions of studied samples (Cho *et al.*, 2013), as would be expected for well-matched CME/ICME pairs (*e.g.* Palmerio *et al.*, 2018). At 1 AU, only about 30% of ICMEs are MCs, but the statistics are generally considered to be influenced by the "observer" sampling of a generally present structure. In particular, only a fraction of the CMEs seen near the solar disk center, which are expected to have a direct impact at Earth, produce local MCs (Gopalswamy *et al.*, 2013a; Jian *et al.*, 2006; Jian, Russell, and Luhmann, 2011; Vourlidas *et al.*, 2013; Li, Luhmann, and Lynch, 2018). In the standard model for the initiation of CMEs, magnetic reconnection within closed, sheared coronal loops forms a flux rope and a post-eruption arcade (*e.g.* Forbes, 2000; Fan and Gibson, 2007). One of the consequences of the reconnection is that the heated plasma enters into the flux rope resulting in the presence of high charge states of minor ions inside MCs when observed at 1 AU (*e.g.* Lepri *et al.*, 2001; Lepri and Zurbuchen, 2004; Reinard, Lynch, and Mulligan, 2012). Analyzing a set of 54 CME–ICME pairs, Gopalswamy *et al.* (2013b) found that MCs and non-MCs were indistinguishable based on their

near-Sun manifestations such as white-light CMEs and post-eruption arcades: the CMEs were fast and the flare arcades were well-defined (Yashiro *et al.*, 2013). Fe and O charge states at 1 AU were also indistinguishable between MCs and non-MCs, suggesting a similar eruption mechanism (Reinard, 2008; Gruesbeck, Lepri, and Zurbuchen, 2012; Gopalswamy *et al.*, 2013a). Furthermore, flux-rope fits to white-light CMEs by Xie, Gopalswamy, and St. Cyr (2013) revealed that MC and non-MC associated CMEs are on average deflected towards and away from the Sun–Earth line, respectively. The different deflections of MC and non-MC CMEs was further confirmed by the different coronal-hole influence parameters for the two groups of CMEs (Mäkelä *et al.*, 2013). Thus, the deflection away from the Sun–Earth line of the non-MC CMEs is consistent with the view that the observing spacecraft often pass through their flanks, missing the central flux-rope structures and resulting in their non-MC appearance (see, *e.g.*, Marubashi, 2000; Owens *et al.*, 2005; Gopalswamy, 2006a; Jian *et al.*, 2006; Jian, Russell, and Luhmann, 2011; Kim *et al.*, 2013). Marubashi *et al.* (2015) showed that almost all ICMEs can be fit with a flux-rope model if a locally toroidal (*e.g.* spheromak) model is also considered in addition to the traditional cylindrical picture. This form may be especially suitable for ejecta crossings far from their centers.

The majority of ICME studies involving heliospheric images has focused on understanding their interplanetary propagation toward determining their direction or forecasting their hit/miss and/or arrival times (Wood and Howard, 2009, Liu *et al.*, 2010; Lugaz *et al.*, 2010; Rouillard, 2011; Wood *et al.*, 2011; Möstl *et al.*, 2014, 2017). A few of these have also tried to take into account their radial expansion (Savani *et al.*, 2009, 2012; Lynch *et al.*, 2010; Nieves-Chinchilla *et al.*, 2012; Lugaz *et al.*, 2012), interplanetary evolution (Poomvises, Zhang, and Olmedo, 2010), and deformation (Savani *et al.*, 2011a, 2011b). Savani *et al.* (2015) projected a reconstructed local structure back onto the solar surface to determine the central axis of the initial CME, its source region, and related coronal magnetic structure, and they compared that information to the *in-situ* ICME magnetic structure detected upstream of Earth. Another method for connecting the magnetic structure of the solar CME to the ICME (Gopalswamy *et al.*, 2018a) is the "flux rope from eruption data" (FRED) technique. This approach infers the total reconnected flux in the eruption region (Qiu and Yurchyshyn, 2005; Qiu *et al.*, 2007; Hu *et al.*, 2014; Gopalswamy *et al.*, 2017a), and then assumes self-similar expansion to 1 AU (Gopalswamy *et al.*, 2018b) to estimate arrival time and predicted Bz-component (Scolini *et al.*, 2019; Singh *et al.*, 2019). In a particularly comprehensive CME image/ICME analysis, Wood *et al.* (2017) focused on the ability to infer the arriving MC's Bz-component sign – essential for geomagnetic-storm predictions. They investigated whether routinely fitting classical croissant-shaped CME flux-rope pictures to multi-perspective coronal and heliospheric images (as illustrated by the magenta field lines in Figure 2), and determining the photospheric fields at their roots, could be used to distinguish the resulting ICMEs that had geo-effectively important southward Bz at 1 AU. Similar techniques have been tested by Kay, Opher, and Evans (2015), Möstl *et al.* (2018), and Palmerio *et al.* (2018). Nieves-Chinchilla *et al.* (2018) and Al-Haddad *et al.* (2019) concluded, as Wood *et al.* (2017) had, that this kind of projection procedure is not widely applicable to connecting the structures observed at the Sun and the magnetic fields of the ICMEs at 1 AU (also see Kilpua *et al.*, 2019).

The most energetic solar-particle events, such as those that produce ground-level enhancement (GLE) events on Earth (Mewaldt *et al.*, 2012), are inferred to have their sources close to the Sun. Thus, there has been significant attention to the question of the onset and evolution of the interplanetary shocks associated with CMEs and ICMEs. This includes the challenge of separating CME and shock structures so that their relationship and consequences can be studied. Their relative 3D evolution affects the interpretation of solar

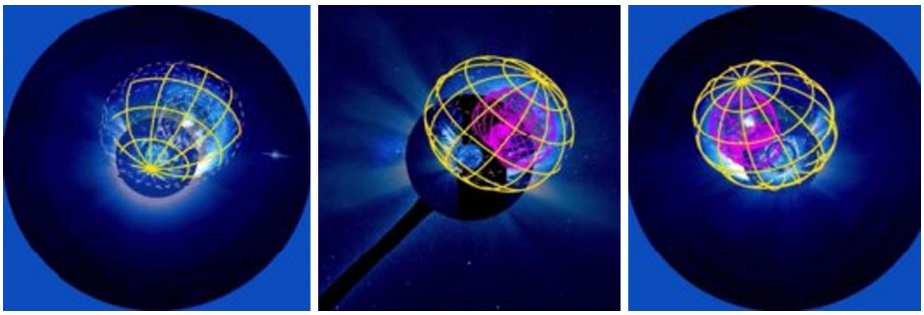

Figure 2 Example illustrating a spherical coronal shock (*yellow grid*) and coronal flux rope (*magenta field lines*) fit to multi-perspective coronal images to interpret, visualize, and empirically model the initial phase of what becomes the ICME in the heliosphere (NASA image).

energetic-particle distributions and intensities throughout the inner heliosphere, as well as the coronal dimmings and EUV waves observed in the low corona (*e.g.* Ma *et al.*, 2011) in conjunction with the early stages of CME-to-ICME transition. Kwon, Zhang, and Olmedo (2014) used SOHO and STEREO's $\approx 360^\circ$ coverage of the corona to investigate the 3D structure of CME-driven shocks and how they are related both to the EUV waves and the CME leading edges in white-light images. A simple geometric representation of the shock as a sphere was found to provide a good description of the coronal disturbance surrounding the erupted material in all three coronagraph viewpoints. This work supported the earlier suggestions that the halo appearance of some CMEs can at times be due to the shocks rather than the CMEs themselves (Shen *et al.*, 2014), and that the EUV wave is the low coronal reaction to the initial expanding CME disturbance (see also Attrill *et al.*, 2007; Downs *et al.*, 2011; Long *et al.*, 2017). In limb events, EUV waves are often interpreted as shock footprints (Veronig *et al.*, 2010; Kozarev *et al.*, 2011; Ma *et al.*, 2011; Patsourakos and Vourlidas, 2012; Gopalswamy *et al.*, 2012a). More recently, Kwon and Vourlidas (2017, 2018) refined the methods of fitting these coronal shocks and extracting information about their strength (*e.g.* their density compression ratios), important to understanding their potential for accelerating solar energetic particles (SEPs) in the corona early in the overall event. The knowledge, from images, of the shock location in the early stages of CME liftoff allows researchers to study the relationship between SEPs arriving at multiple heliospheric locations and their coronal source as done by Rouillard *et al.* (2011) and Lario *et al.* (2014, 2016, 2017). Those authors found mixed results in using observer field-line backward mapping to the coronal-shock signatures, but the insights gained regarding both the interpretations of the observations close to the Sun and their connections to what is observed at 1 AU are important.

The detectability of high-energy particles at a given observer location (*e.g.* associated with a GLE) may depend on its magnetic connectivity to the nose of the shock (where it is expected to be strongest) determined from images of the early stages of CMEs in white light or EUV (Gopalswamy *et al.*, 2014a, 2016). When STEREO observations with the extended coronagraph field of view close to the solar surface (STEREO/COR1) are available together with EUVI images, it is possible to accurately determine the shock-formation height (Gopalswamy *et al.*, 2009c, 2013d): an important parameter to determine the particle acceleration efficiency of CME-driven shocks (Gopalswamy *et al.*, 2017b). The shock formation depends on the relative importance of the Alfvénic (or magnetosonic) speed profile in the corona and the CME-speed profile (Gopalswamy *et al.*, 2001c; Mann *et al.*, 2003). As mentioned earlier, in GLE events, the inferred shock-formation height

is typically around 1.5 $R_\odot$ (Gopalswamy *et al.*, 2013e, 2018c; Thakur *et al.*, 2014) and is consistent with the velocity dispersion analysis of GLE SEPs (Reames, 2009). On the other hand, the shock-formation height is much larger (about 5 – 10 $R_\odot$) in the case of accelerating CMEs associated with filament eruptions outside of active regions (*e.g.* Kahler, 2001; Gopalswamy *et al.*, 2015c, 2016, 2017b). The particle-acceleration efficiency is also determined by the speed of the CME at the shock-formation height. If the shock-formation height is low and the CME speed is also low, then one gets only small SEP events (Gopalswamy *et al.*, 2017b). If the observer is connected to the weaker shock flank, the resulting particle spectrum becomes softer (Gopalswamy *et al.*, 2018c).

The coronal shock is expected to form at a stage when the CME/ICME evolution is dominated by the heating and magnetic-pressure-induced expansion associated with the combined flare and CME eruption, and it weakens as the local effects subside. As the expanding ejecta move outward, the less-symmetrical driven shock takes over. The evolution of the shock standoff distance is an indication that the driving CME slows down with distance from the Sun (Gopalswamy and Yashiro, 2011). Its efficiency as an SEP source is not determined, although SEPs may also be accelerated in the flare and eruption processes. But the "driven" shock can be maintained by the outwardly moving and expanding ejecta from the corona to large radial distances and is a source for large "gradual" SEP events that can last several days up to, and beyond, the ICME shock arrival time at 1 AU (Cohen, 2006; Mäkelä *et al.*, 2011; Reames, 2017). As already mentioned, GLE timing suggests that the shock must already have formed at less than 10 $R_\odot$ heliocentric distance, which seems to be the case for large SEP events in general (Ma *et al.*, 2011; Kozarev *et al.*, 2015; Gopalswamy *et al.*, 2017b). Note that some driven shocks identified near the Sun using Type-II burst observations may not arrive at 1 AU for various reasons (Gopalswamy, 2006b; Gopalswamy *et al.*, 2012b). The driving CMEs are of lower energy, so the shocks may dissipate before arriving at Earth, or closely spaced and timed CME shocks may merge, resulting in a single shock at Earth (Schmidt and Cargill, 2004; Lugaz, Manchester, and Gombosi, 2005), or deflection of the shock driver or the shock itself, away from their original Sun–Earth line trajectory by nearby coronal and solar-wind structures may occur. However, the probability of observing the shock at 1 AU increases rapidly when the imaged CME speed exceeds 1000 $km\,s^{-1}$ and when the Type-II bursts are observed down to frequencies below 1 MHz. Radio observations of particle acceleration regions around CMEs are still increasing in their capability (*e.g.* Zucca *et al.*, 2018; Morosan *et al.*, 2019), and are expected to reveal further details of where and when CME and ICME related sources become important.

The present Cycle 24 solar activity went through its (comparatively weak) maximum in $\approx$ 2011 – 2014 (*e.g.* Gopalswamy *et al.*, 2015b) when the multipoint, multi-perspective observational resources provided by L_1 and STEREO spacecraft were all available. During this period, it became better appreciated that the larger, faster CMEs can occur in quick succession and can also be accompanied by lesser eruptions (Möstl *et al.*, 2012; Lugaz *et al.*, 2012; Gopalswamy *et al.*, 2013c; Liu *et al.*, 2014a, 2014b; Temmer *et al.*, 2014), confirming findings made with LASCO during Solar Cycle 23 (Gopalswamy *et al.*, 2001a). As a result, the possibility of CMEs interacting in the inner heliosphere significantly increases. CME–CME interactions are important both because they affect CME/ICME propagation and evolution, and, from a space-weather point of view, because the resulting geomagnetic and SEP effects can be greatly altered (see review by Lugaz *et al.*, 2017a). SOHO and STEREO studies of interacting CMEs, with the addition in 2010 of the *Solar Dynamic Observatory* (SDO)'s EUV imaging capabilities, have taken advantage of the combined solar observations and separated *in-situ* measurements to understand their detailed characteristics. For example,

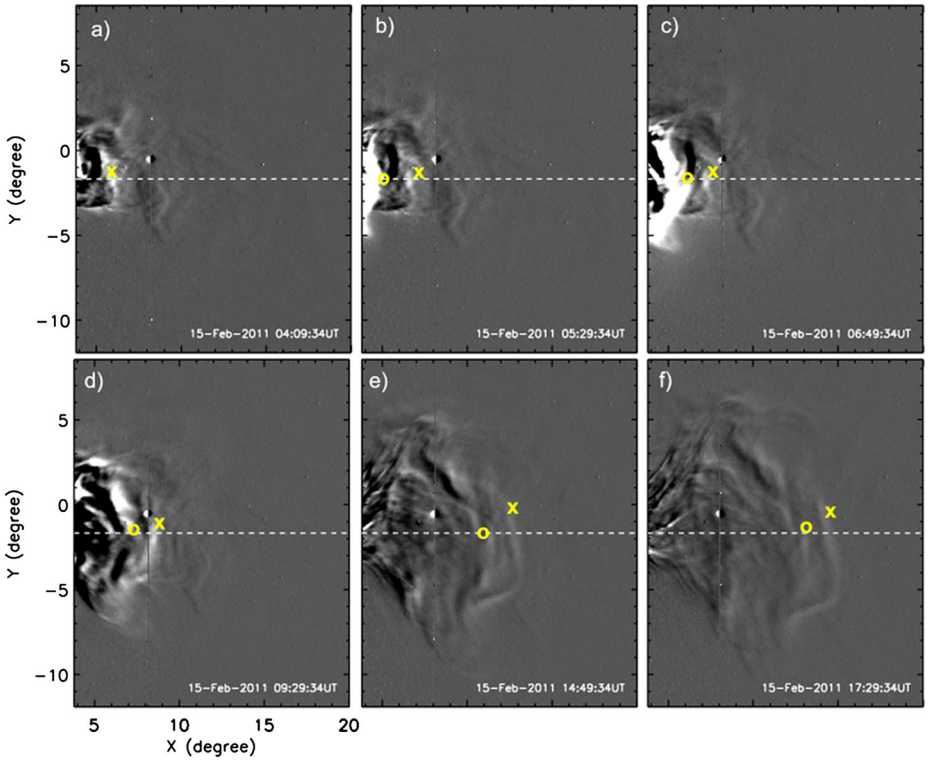

Figure 3 STEREO/HI images of three CMEs merging near the Sun and propagating outward as a complex structure. The *dashed line* is the Ecliptic. The o- and x-points mark leading-edge features of two of the original events. (Image reproduced with permission from Maricic *et al.* (2014), copyright by Springer.)

Figure 3 (from Maricic *et al.*, 2014) shows an example where HI observations recorded the merging of three CMEs near the Sun that eventually impacted the Earth and caused a single complex response. STEREO observations of Earth-directed CMEs revealed small CMEs preceding SOHO/LASCO halo CMEs that helped explain the altered ICME travel times (Gopalswamy *et al.*, 2013c). Webb *et al.* (2013) described the complicated structure of the inner heliosphere during a very active period in early August 2010, an interval that was also the subject of dedicated studies and publications (Temmer *et al.*, 2012; Harrison *et al.*, 2012; Möstl *et al.*, 2012). Some authors reconstructed 3D heliospheric densities from the images and compared them with the timing and magnitude of *in-situ* density structures at five spacecraft locations spread over 150° in ecliptic longitude and 0.4 to 1 AU in radial distance, together with modeled local flux-rope structures (Webb *et al.*, 2013). This work highlighted the difficulties in using kinematics to describe the morphological evolution of ICMEs during periods of widespread activity. Many of the intense geomagnetic storms from Solar Cycle 24 resulted from the succession or interaction of CMEs (Gopalswamy *et al.*, 2015b; Lugaz *et al.*, 2016; Shen *et al.*, 2018). CMEs and ICMEs always interact with ambient flows of different origins as they propagate from the corona into the interplanetary medium. White-light image-based "J-maps" suggest that interaction with large-scale structures close to the Sun, including coronal streamers, coronal holes, solar-wind stream boundaries, and other CMEs, can severely alter the shapes and trajectories of the coronal ejecta and affect the ICMEs they evolve into. Their ongoing interactions during ICME propagation impact

the plasma and field parameters associated with the arriving plasma and field disturbance(s), and the associated SEPs.

The physical details of the encounters between CMEs/ICMEs is complicated and determines whether their interaction is constructive, destructive, or neutral. A recent review of the subject by Lugaz *et al.* (2017a) discusses a number of examples and studies. Early work based on heliospheric images (Shen *et al.*, 2012; Lugaz *et al.*, 2012) found evidence of both deflection of one CME/ICME by another and of super-elastic collisions, in which momentum redistribution occurs in ways that enhance the event. Several investigations examined the kinematics of ICME interactions to determine the manner in which they merge. Maricic *et al.* (2014) described a chain of events on 14 – 15 February 2011 and found evidence for a gradual momentum transfer from the faster to the slower CME ahead. They inferred that momentum transfer may result from alteration of the following events' shock propagation as they travel through the preceding events. This was interpreted as causing additional drag on the faster ICMEs, resulting in deviations from expected travel times (see also Gopalswamy *et al.*, 2013c). Temmer *et al.* (2014) presented a detailed analysis of the interaction of two of these CMEs. It was found that the interaction process strongly depends on the geometry, with differences in the outcome for interacting ICME flanks *versus* apexes, and the most centrally located interaction showing the strongest changes in kinematics. This topic was also addressed by Mishra and Srivastava (2014), who described evidence in the *in-situ* observations near 1 AU of acceleration, compression, and heating of the leading ejecta. Mishra, Wang, and Srivastava (2016) studied a case involving two interacting CMEs that occurred on 25 October 2013. They considered the propagation and expansion speeds, impact geometry, angular sizes, and masses of the interacting CMEs using 3D-reconstruction techniques applied to STEREO/SECCHI-COR and -HI observations, and they found that the higher expansion speed of the following CME compared to the preceding CME may increase the probability of interaction. In general, interactions with their surroundings can seriously affect both the initial state and evolution of ICMEs in the interplanetary medium. In particular, when there are small-to-moderate CMEs ahead of a large CME that is potentially geo-effective, the arrival time of the larger ICME can be significantly altered relative to the expected time based on the coronal observations. One attempt has been made to develop an analytical model to determine where CMEs interact near the Sun, and the consequences for their arrival time at Earth (Niembro *et al.*, 2015). The approach was tested on several real events, with results that seemed to depend on how well they could be described and tracked. However, just the knowledge that there have been significant interactions can be important in both event interpretations and space-weather forecasting.

An exceptionally fast and large CME seen as a halo event on STEREO-A when the spacecraft was about 120° ahead of Earth on 23 July 2012 inspired excitement in part due to its occurring during the relatively weak Solar Cycle 24. Its near-Sun speed, at upwards of $\approx 2500\,\mathrm{km\,s^{-1}}$, was at the high end of observed CME speeds. The event also gave rise to an exceptionally intense SEP event detected by STEREO-A (Russell *et al.*, 2013), where the leading shock of the ICME was likely eroded by the significant local pressure contribution from the large density of SEPs. The question of how such extreme space-weather storms are born and evolve, and how severe they can be when they reach Earth, was examined by Liu *et al.* (2014a), where the authors investigated this period using multi-point remote-sensing and *in-situ* observations. At least three effects of multiple-event interactions were found to influence what was observed: i) deflections in the propagation direction of the fastest CME/ICME leading to a head-on impact with STEREO-A, ii) extreme compressions of the ejecta magnetic fields to over 100 nT, and iii) minimal deceleration during the Sun-to-STEREO-A transit due to a prior event having left a rarefied ambient solar wind in its

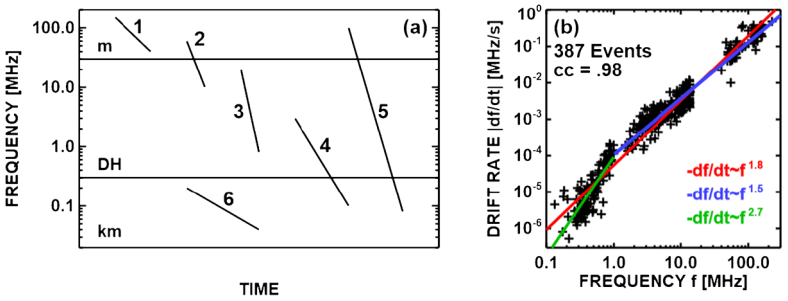

Figure 4 (**a**) Type-II bursts occur at different wavelength ranges, as illustrated here: 1. purely metric, 2. metric to DH, 3. DH, 4. DH – kilometric, 5. metric to kilometric, and 6. purely kilometric. (**b**) The drift rate $[\mathrm{d}f/\mathrm{d}t]$ dependence on the emission frequency $[f]$ in the m, DH, and km domains using data from various sources (from Gopalswamy, 2011) indicates whether the source is accelerating or decelerating.

wake (Liu *et al.*, 2014a; Temmer and Nitta, 2015). Together, these caused an unprecedented set of interplanetary conditions, including an extended period of strong southward magnetic field (-Bz) which, had it arrived at Earth, would have produced a record geomagnetic storm. Gopalswamy *et al.* (2016) compared the 10 – 100 MeV proton spectrum of this event with other large SEP events and found that the 23 July 2012 event was similar to those with GLEs, meaning that GeV particles were likely accelerated. This result also implies that the CME attained very high speeds close to the Sun. These results provided new insights on how an extreme space-weather event can arise from a combination of conditions and events both at the Sun and during propagation to 1 AU.

3. ICME Radial Evolution: As Revealed by Radio Emissions

Solar radio emissions provide a unique remote-sensing diagnostic of the CME process, and its related shock generation and propagation. One of the radio burst types closely related to the occurrence of CMEs is the Type-II burst (see Nelson and Melrose, 1985, for a review). Type-II bursts have been observed in the frequency range from 100s of MHz to tens of kHz (Cane and Stone, 1984; Cane, Sheeley, and Howard, 1987; Gopalswamy *et al.*, 2012a; Cho *et al.*, 2013). From a plasma-frequency perspective, these frequencies span the spatial domain starting from the inner corona to the vicinity of observing spacecraft at L_1, and occasionally even further. This provides the opportunity to track shocks throughout the inner heliosphere starting from about 1.1 $R_\odot$ to > 215 $R_\odot$ (*e.g.* Gopalswamy, 2011; Liu *et al.*, 2013; Cremades *et al.*, 2015). When the *Radio and Plasma Wave Experiment* (WAVES: Bougeret *et al.*, 1995) onboard the *Wind* spacecraft became available, observations in the decameter–hectometric (DH) wavelength domain led to important discoveries regarding CME interactions (Gopalswamy *et al.*, 2001a) and the establishment of the relationship between CME kinetic energy and the wavelength range over which the radio emission takes place (Gopalswamy *et al.*, 2005).

Figure 4a shows a schematic dynamic spectrum with the slanted lines indicating Type-II bursts in various wavelength ranges. Some Type-II bursts start and end in the metric domain; some start in the metric domain and continue to be present in the kilometric domain. There are also intermediate cases. Finally, some bursts start in the kilometric domain. The Type-II wavelength range provides important information about the CME kinematic evolution in the corona and interplanetary (IP) medium. Purely metric Type-II bursts are associated with

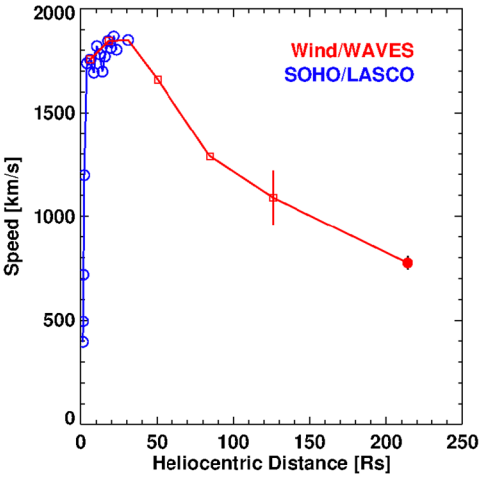

Figure 5 Sun-to-Earth evolution of a shock associated with the 21 June 2015 CME. SDO and SOHO observations provided the open circles, while the squares are from the *Wind*/WAVES radio dynamic spectrum. The *in-situ* shock speed at L_1 from *Wind* (776 km s^{-1}) is shown by the *solid circle*. (Image reproduced with permission from Gopalswamy *et al.* (2018d), copyright by Elsevier.)

CMEs that have an average speed of ≈ 600 km s^{-1}. CMEs producing Type-II bursts in the DH domain have an average speed of ≈ 1100 km s^{-1}. Type-II bursts with emission components at all wavelengths (metric, DH, and kilometric) are produced by the fastest CMEs (≈ 1500 km s^{-1}) (Gopalswamy, 2011). CMEs producing purely kilometric Type-II bursts have the lowest average speed (≈ 550 km s^{-1}), only slightly smaller than that of CMEs associated with metric Type-II bursts. All CMEs, except those associated with kilometric Type-II bursts, have an average deceleration in the coronagraph field of view. CMEs associated with the kilometric Type-II bursts have average positive acceleration and attain super-Alfvénic speeds at several tens of solar radii from the Sun where they form shocks, and they produce the radio emission at long wavelengths. The slope of the lines [df/dt] in Figure 4a is related to the shock speed and the density scale height. The burst drift-rate spectrum (Figure 4b) provides a picture of the shock evolution from the corona to the interplanetary medium. In the inner corona, the drift-rate spectrum is flat, indicating an accelerating source, while in the interplanetary medium, the drift-rate spectrum is steep, indicating deceleration (see Gopalswamy, 2011, for details).

In a recent work, Gopalswamy *et al.* (2018d) tracked the shock speed from the corona to IP medium, using a well-observed Type-II burst during the 21 June 2015 CME, which produced the second largest geomagnetic storm in Cycle 24 and a large SEP event (Liu *et al.*, 2015). The Type-II emission was observed from metric to kilometric wavelengths. The 3D speed of the CME was determined by fitting a flux rope to the SOHO/LASCO observations. The leading-edge speed of the CME was tracked in the coronal images and using the Type-II burst that was also observed near the *Wind* spacecraft when the shock arrived. The drift rate of the Type-II burst was determined at several heliocentric distances and the shock speed was derived. The combined coronagraph, Type-II burst, and *in-situ* observations provided the complete record of the evolution of the shock speed from the Sun to Earth shown in Figure 5. The combined data set captured the complete evolution: the initial rapid increase, slow increase in the outer corona, rapid decline within ≈ 100 $R_\odot$, and finally a slower decline until the shock was detected *in situ* by the *Wind* spacecraft. Using the CME images, it was also possible to deduce that the metric Type-II emission originated from the flanks of the shock approximately 60° from the nose, while the IP Type-II burst originated from the nose region of the shock. This example demonstrates how the radio signatures of ICME shocks can provide substantial and unique additions to what is obtained from the imaging observations regarding the evolution scenario interior to 1 AU.

In a study involving 222 IP shocks detected by *Wind* and/or *Advanced Composition Explore*r (ACE), Gopalswamy *et al.* (2010) found that about $\approx 34\%$ lacked Type-II radio bursts (radio-quiet or RQ shocks). The CMEs associated with the RQ shocks were generally slow (average speed ≈ 535 km s^{-1}) compared to those associated with radio-loud (RL) shocks (average speed ≈ 1237 km s^{-1}). The average Sun-to-Earth transit speeds of RQ and RL shocks were 629 km s^{-1} and 851 km s^{-1}, respectively. This is consistent with the lower CME kinetic energy associated with RQ shocks. CMEs associated with RQ shocks were generally accelerating within the coronagraph field of view (average acceleration $\approx +6.8$ m s^{-2}), while those associated with RL shocks were decelerating (average acceleration ≈ -3.5 m s^{-2}). This means that many of the RQ shocks formed at large distances from the Sun, typically above 10 $R_\odot$, consistent with the absence of metric and DH Type-II radio bursts. A Type-II burst starting at a frequency of 300 kHz (1 km wavelength) indicates that the shock forms at a distance of ≈ 20 solar radii as inferred from a simple density model (*e.g.* Leblanc, Dulk, and Bougeret, 1998). Longer-wavelength bursts imply shock formation at even larger distances from the Sun. The Alfvénic Mach numbers of RQ shocks at 1 AU average 2.6 compared to 3.4 for RL shocks, suggesting that RQ shocks were mostly subcritical, so they were not efficient in accelerating electrons (hence radio quiet). About 18% of the *in-situ* shocks studied do not have discernible ejecta behind them. These shocks are probably due to CMEs moving at large angles from the Sun–Earth line as mentioned in the earlier discussion of observer sampling geometry, although some could also be associated with solar-wind stream interaction regions. As with all of the observing techniques discussed here, the overall event geometry relative to the observer determines how much information can be extracted.

Radio enhancement signatures associated with CME interactions provide another opportunity, in addition to the images, to diagnose these occurrences with remote sensing. These have been interpreted as the signature of the acceleration of additional electrons (Gopalswamy *et al.*, 2001a). Mäkelä *et al.* (2016) were able to identify the location of this acceleration using the direction-finding technique from STEREO and WAVES observations. The interacting CMEs on 2 May 2013 observed by SOHO and STEREO had a radio-enhancement source that was located at the interface between the two interacting CMEs. It has been argued that the same may be happening for protons: major SEP events may result from these CME interactions occurring close to the Sun where the CME-driven shocks are the strongest (*e.g.* Gopalswamy *et al.*, 2002, 2004; Li *et al.*, 2012). Recently, Ding *et al.* (2019) studied 64 radio-enhancement events and the associated SEP events from Solar Cycle 24. They confirmed that the radio-enhancement signature is the key difference between SEP-rich and SEP-poor eruptions, as suggested by Gopalswamy *et al.* (2002). This is another piece of information that complements the imaging information toward inferring what is happening as the ICME evolves close to the Sun.

4. ICME Radial Evolution: As Revealed by *In-Situ* Measurements

The *in-situ* features of ICMEs have been analyzed by many authors whose goals have ranged from understanding the structure of these interplanetary disturbances, to making connections to their solar counterparts, to considering their role as the external drivers of geomagnetic storms. Figure 6 contains examples of the 1 AU *in-situ* signatures of a few large ICMEs observed in the STEREO era, including the plasma, magnetic field, and SEPs (also see Jian *et al.*, 2006, 2018d). Although the 1 AU measurements, like the coronal images, indicate the presence of erupted coronal material (including magnetic-flux ropes) preceded

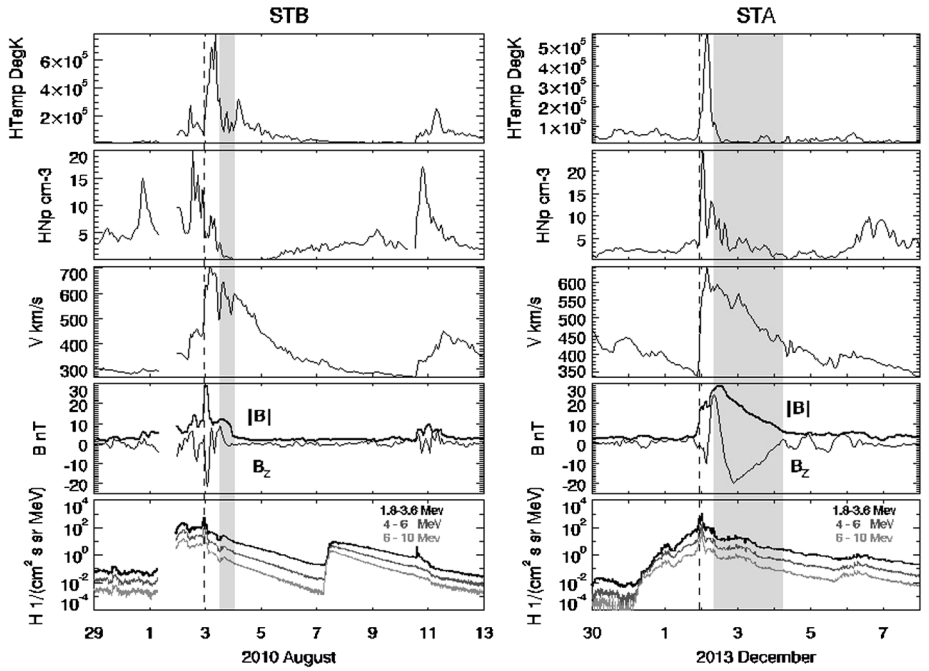

Figure 6 Examples of ICMEs observed with *in-situ* instrumentation on STEREO. The panels show (*from top to bottom*) proton temperature, density (both showing the ICME sheath compression and heating of solar wind at the leading shock marked by *dashed lines*), plasma velocity, magnetic-field magnitude, and north–south (Bz) component showing the enhancement and rotations associated with the magnetic-cloud driver, and the SEP protons that are the first arriving *in-situ* signature.

by a shock (for fast-moving cases) and sheath, their relationship to what is observed at the Sun is not totally clear (*e.g.* Dasso *et al.*, 2007; Manchester *et al.*, 2017 and the references therein). Focusing on the 1 AU ICMEs associated with observed CMEs, Möstl *et al.* (2014) examined 22 events seen both at the Sun and in heliospheric images, and at various 1 AU locations, to give a more comprehensive empirical picture of how the kinematics, directions, and global shapes of ICMEs change during propagation from the Sun. Li, Luhmann, and Lynch (2018) similarly analyzed the relationships between a large selection of *in-situ* events that had magnetic-cloud drivers, identifying the solar signatures that seemed to be most closely related – including flares, filament eruptions, and "stealth" types of sources, where no solar counterpart could be identified in the latter (*e.g.* Howard and Simnett, 2008). Nieves-Chinchilla *et al.* (2013) used joint *in-situ*/imaging observations to study the 3D evolution of a particular stealth CME in detail. An important finding in several of these studies was that the errors of hours, and sometimes days, in expected arrival times based on the coronal CME time and speed was difficult to account for, with possible contributors including the history of interactions with ambient structures and the assumed shape and flux content of the propagating driver. On the other hand, He *et al.* (2018) tracked the 8 October 2016 stealth CME with SDO, SOHO, STEREO, and *in-situ* observations, and, using additional modeling, they were able to infer that the stealth CME was bracketed between slow solar wind ahead and a fast stream behind. In general, an essential part of interpreting what is observed is understanding the surrounding plasma and field context of the event, and its physical interactions with those surroundings as it travels (also see Farrugia *et al.*, 2011).

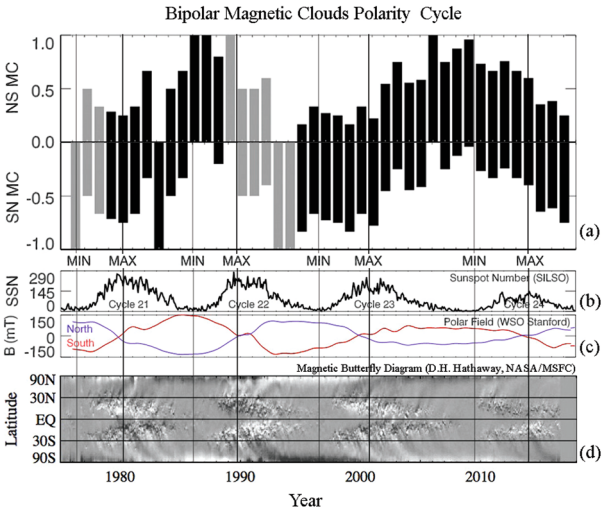

Figure 7 Results from analyzing the magnetic "polarity" (north–south or Bz magnetic field) of several decades of *in-situ* observations of ICME magnetic-cloud drivers. The clear solar-cycle trends in the occurrence rates of magnetic clouds with leading northward (NS) and leading southward (SN) magnetic-field rotations are seen here, including the effect of the solar polar-field polarity on which dominates. Adapted from Li, Luhmann, and Lynch (2018).

Processes referred to as drag and/or erosion (*e.g.* Ruffenach *et al.*, 2012, 2015) are often not explicitly considered in event analyses, and are still poorly understood. These studies represent only a small fraction of recent work on *in-situ* studies of ICMEs. Many others are described in the comprehensive review by Kilpua, Koskinen, and Pulkkinen (2017) and the references therein.

The solar-cycle dependence of ICMEs has been well-documented. Although their occurrence rate trends are not always a reflection of the related sunspot-cycle sizes, during the relatively weak Solar Cycle 24 ICMEs have occurred less often and have been generally weaker and slower than in the previous cycle (Gopalswamy *et al.*, 2015b; Chi, Shen, and Wang, 2016; Jian *et al.*, 2018d). Fewer CMEs were also seen in the coronal observations by Hess and Colaninno (2017), especially the fast and wide ones that usually result in easily identifiable ICMEs. Gopalswamy, Tsurutani, and Yan (2015) suggested this decrease in ICME numbers was not solely due to propagation differences and/or ICME size and identification issues. Although the mean speeds of the CMEs close the Sun are similar for Cycles 23 and 24 (Gopalswamy *et al.*, 2014b), the measured ICME speeds at 1 AU in Cycle 24 are slower. Reduced total pressures near the Sun, where coronal densities and fields have diminished relative to earlier cycles, may have allowed the Cycle 24 CMEs to expand more quickly close to the Sun (Gopalswamy *et al.*, 2015a), while the ICME widths at 1 AU decreased (Jian *et al.*, 2018d). One also cannot rule out a possible *in-situ* sampling bias in the impact parameter that is different for the two cycles, perhaps due to greater average deflection of the eruptions from the ecliptic plane (*e.g.* Kay, Opher, and Evans, 2015).

The MCs mentioned earlier represent a significant subset ($\approx 30\%$) of observed ICMEs at 1 AU, especially during less active periods surrounding solar minimum (*e.g.* Richardson and Cane, 2004). As a major factor affecting the related geomagnetic activity, the north–south or Bz-component of these ejecta exhibit bipolar (Bz changes sign) and unipolar (Bz does not change sign) configurations when the axis of the flux rope is oriented at low *vs.* high inclinations with respect to the ecliptic plane, respectively (*e.g.* Mulligan, Russell, and Luhmann, 1998; Gopalswamy, 2008). Li *et al.* (2014) and Li, Luhmann, and Lynch (2018) have made long-term analyses of the solar-cycle trends in the polarity of bipolar MCs, defined as the time-ordering of the rotation, which varies with the Hale cycle as illustrated in

Figure 7. While bipolar MCs show a clear inter-cycle variation, the unipolar MCs do not show such a variation, at least in Solar Cycle 23. However, Li, Luhmann, and Lynch (2018) and Nieves-Chinchilla *et al.* (2019) found there were more unipolar MCs at solar maxima although the preference of north or south orientation does not have any clear solar-cycle dependence. From Solar Maximum 23 to Solar Maximum 24, the NS (north to south) MCs dominated, and presently the SN (south to north) MCs dominate (Li, Luhmann, and Lynch, 2018; Nieves-Chinchilla *et al.*, 2019). Li, Luhmann, and Lynch (2018) found the solar-cycle dependence of the bipolar MC average polarity is attributable to MCs that originate from quiescent filaments in decayed active regions, while those associated with flaring active-regions have mixed Bz polarity without solar-cycle dependence.

Significant progress on the subject of ICME transport and evolution was made possible over the maximum of Solar Cycle 24 by the solar-activity level and the availability of spacecraft at various locations in both radius and helio-longitude: *MErcury Surface, Space ENvironment, GEochemistry, and Ranging* (MESSENGER) at ≈ 0.3 AU, *Venus Express* at ≈ 0.7 AU, and *Wind*, ACE, SOHO, SDO, and STEREO with its dual, separated perspectives at 1 AU. In particular, the multipoint *in-situ* observations from 0.3 to 1 AU and multi-perspective images from 1 AU provided an essential link for interpreting solar-system-wide evolution and consequences of both solar-wind structure and ICMEs. STEREO often provided the closest 1 AU location for *in-situ* data comparison for planetary missions because of its longitudinal separation from the Sun–Earth line. For the first time since the mid-1980s with the *Helios* mission, MESSENGER provided *in-situ* measurements (although with limited plasma data) at heliocentric distances of less than 0.5 AU, often within the field-of-view of STEREO's *Heliospheric Imagers*. In addition, the relatively fast orbit of Mercury (88-day orbital period) resulted in many potential conjunction events with solar-wind monitors near 1 AU (*Wind*/ACE and STEREO).

Planetary scientists have made a wide variety of uses of the distributed heliospheric measurements to interpret space-weather conditions at Mercury, Venus, Mars, and beyond including studies of the radial evolution of these transient structures. Winslow *et al.* (2015) assembled a list of ICMEs that impacted MESSENGER while it orbited Mercury (2011 – 2015). They found that the average ICME expansion between 0.3 and 1 AU was very similar during Solar Cycle 24 to that inferred from *Helios* measurements during Solar Cycle 21. They then used STEREO and L_1 data together with MESSENGER observations to evaluate the statistical differences in ICME strengths between the orbital distances of Mercury and Earth. Their analysis also showed the overall weakening of most leading shocks, consistent with an average deceleration of the ejecta drivers in that heliocentric-distance range. In another study, Winslow *et al.* (2016) used conjunctions of STEREO-A and MESSENGER to investigate the development of complexity during the propagation of several ICMEs between the two locations, although Good *et al.* (2015) had found that some events simply expand self-similarly over this radial range. The ambient conditions, *e.g.* whether significant solar-wind stream structure and/or the heliospheric current sheets are present, appear to influence the outcome. Good and Forsyth (2016) assembled a catalogue of MESSENGER ICMEs covering its seven-year transit to Mercury with *Venus Express* (VEX), STEREO, and ACE event data, enabling the determination of ICME widths at different radial distances and their consistency with self-similar expansion (Good *et al.*, 2019). They identified 23 ICMEs observed by pairs of spacecraft in close radial alignment, providing a valuable resource to those seeking to analyze the differences in space weather at the terrestrial planets and the heliospheric contexts of events occurring during the MESSENGER and VEX missions (2006 – 2013). A study that incorporated both *Mars Science Laboratory* (MSL)/*Radiation Assessment Detector* (RAD) and *Mars Express* data (Möstl *et al.*, 2015) used STEREO observations to model the direction and expansion of a Sun-to-Mars event, concluding that

non-radial propagation can be significant. Witasse *et al.* (2017) presented a case study that may have included ICME detection as far out as Saturn, by the *Cassini* spacecraft, and at *New Horizons en route* to Pluto. However, the level of detail derivable from the collection of observers in this case mainly makes the point that those ICMEs that propagate well beyond 1 AU can still be identified with a particular solar event. Jian *et al.* (2006, 2008a, 2008b) and Jian, Russell, and Luhmann (2011) conducted a number of analyses focusing on determining the changing properties of ICMEs at Venus, Earth, and Jupiter orbital distances using *Pioneer Venus Orbiter* (PVO), *Wind*/ACE, and *Ulysses* data, respectively, with sufficient events in each location to determine solar-cycle variations. Their results show that, as the ICMEs propagate away from the Sun, they increasingly interact with other ICMEs or solar-wind stream interaction regions, with the fraction as high as 37% at 5.3 AU (Jian *et al.*, 2008b). From 1 to 5.3 AU, the occurrence of ICME shocks decreases slightly and the expansion rate of the ICME drivers is less than it is within 1 AU (Jian *et al.*, 2008b).

Most recently, Janvier *et al.* (2019) derived average properties and magnetic-field temporal profiles of ICMEs for Mercury, Venus, and Earth heliocentric distances from the collected observations, finding radial trends that generally agree with the conclusions of the multipoint case studies, but also adding insight regarding evolution of observed asymmetry in the ICME temporal profile. As asymmetries are affected by impact parameter sampling of the passing structure, which can introduce apparent asymmetry, interpretation is challenging. Asymmetries can also result from propagation effects. Dasso *et al.* (2006) pointed out that magnetic reconnection at the front and/or rear edges of ICME flux ropes would reduce the magnetic flux of a flux rope and alter its observed polarity pattern. Ruffenach *et al.* (2015) selected 50 MCs and found that nearly 30% of them showed potential reconnection signatures at their boundaries, with average erosion of about 40% of the total azimuthal magnetic flux. It is clear that the ICME propagation and evolution processes, as well as sampling considerations, make it difficult to interpret *in-situ* observations in a straightforward way.

A topic of special interest in space-weather forecasting concerns the ability of the ICMEs to drive shocks and the heliocentric distance of shock formation. ICME ejecta both expand and propagate, leading to shock formation in cases where they do so with super-magnetosonic speeds relative to the background plasma (Siscoe and Odstrcil, 2008). In the corona, strong events can accelerate particles within mere minutes after their initiation (*e.g.* Gopalswamy *et al.*, 2012c). On the other hand, there are, on average, more CMEs with shocks at 1 AU than at 0.7 AU, from 48% to 65% although this result comes from analyses of long-term observations obtained during different solar cycles (Jian *et al.*, 2008a, 2008c). As mentioned earlier, radio-quiet shocks (Gopalswamy *et al.*, 2010; Janvier, Démoulin, and Dasso, 2014), and shocks with purely kilometric Type-II bursts (Gopalswamy *et al.*, 2005) are known to form at large distances from the Sun and hence may provide an explanation for the higher abundance of shocks at 1 AU. Measurements at 1 AU (Lugaz *et al.*, 2017b) and numerical simulations (Poedts, Pomoell, and Zuccarello, 2016) indicate that slow CMEs may be able to drive shocks in part due to their large and long-lived expansion. It is unclear yet where these shocks form, as it depends on the relative decrease with radial distance of the ambient coronal and solar-wind plasma parameters, the solar-wind fast magnetosonic speed, and the CME (ejecta) speed including its expansion speed. The observed occurrence of ICME leading shocks at 1 AU varies in phase with solar activity and is on average about 65% (Jian, Russell, and Luhmann, 2011; Jian *et al.*, 2018d). The magnetosonic Mach number of these shocks is generally 1.2 to 4. Kilpua *et al.* (2015) found little solar-cycle variation in these numbers, suggesting that the combination of ICME and solar-wind properties both change in such a way as to maintain this general

range of shock strengths. Using *Helios* 1/2 data, Lai *et al.* (2012) studied the radial variation of the magnetic-field compression ratios of 50 quasi-perpendicular shocks from 0.3 to 1 AU, as a proxy for the radial variation of Mach number, finding that the Mach number of ICME shocks does not vary much with heliocentric distance.

The shocks driven by ICMEs often have large proton foreshocks, regardless of whether the shocks are quasi-perpendicular or quasi-parallel (Blanco-Cano *et al.*, 2016). The foreshocks can range in upstream extent to more than 0.1 AU, relatively greater than their planetary bow-shock counterparts. This may be due to the shocks forming close to the Sun that then energize particles for longer times as they propagate to 1 AU. MESSENGER, with its SEP-detection capability, provided opportunities to evaluate the radial dependence of peak SEP intensities, an indirect diagnostic of CME and ICME shocks. For a selected set of events, MESSENGER was lined up along the interplanetary spiral field with one of the distributed 1 AU spacecraft. Lario *et al.* (2013) studied the radial and longitudinal distribution of ≈ 100 keV SEP electrons using MESSENGER, STEREO, and ACE data. They found a radial falloff of the peak SEP intensity significantly greater than the R^{-3} dependence expected from theory. In general, the SEP part of the ICME greater consequences is also tied to the overall understanding of its onset and evolution.

5. ICME Radial Evolution: As Revealed by Numerical Simulations

The past decade has seen multiple developments with respect to numerical simulations of CMEs and ICMEs including the routine usage and further development of models appropriate for real-time forecasting, Sun-to-1 AU simulations capable of producing synthetic observations (EUV, coronagraphs, HI, and/or *in situ*), and coronal simulations of complex initiation mechanisms, with the results sometimes extended all the way to 1 AU.

Heliospheric MHD codes such as ENLIL (Odstrcil, 2003; Odstrcil, Pizzo, and Arge, 2005; Odstrcil and Pizzo, 2009) are now used in real-time for space-weather forecasting but also as support for research, especially to visualize and follow ICME heliospheric propagation and determine which ICMEs may impact a planet or interplanetary spacecraft. ENLIL results feature a solar wind based on inner heliospheric boundary conditions at 21.5 $R_\odot$ from the semi-empirical Wang–Sheeley–Arge (WSA) model (Arge and Pizzo, 2000) or at 30 $R_\odot$ from the MHD-Algorithm-outside-a-Sphere (MAS) coronal model with polytropic and thermodynamic versions (*e.g.* Lionello, Linker, and Mikic, 2009; Lionello *et al.*, 2013). The WSA model uses solar-surface-field synoptic maps constructed from magnetograph observations, together with a modified potential-field source-surface (PFSS) coronal-field model, to provide a first-order description of the initial stream structure and interplanetary field. Aspects of the ICME transients are included by applying the so-called "cone model" in which a (typically conic-section shaped or spherical) high-pressure pulse with direction, location and speed based on coronagraph images of CMEs is introduced into the simulation at its inner boundary (*e.g.* Mays *et al.*, 2015). ENLIL has proven to be a broadly useful tool for interpreting widespread *in-situ* measurements of ICMEs. For example, the WSA-ENLIL+Cone model was used to produce simulated ICME "shocks" whose arrival times at different planetary and spacecraft locations were compared with *in-situ* observations (*e.g.* at Earth by Bain *et al.*, 2016, at Venus by Möstl *et al.*, 2018, at Mercury by Baker *et al.*, 2013, and at Mars by Lee *et al.*, 2017). Most often, models such as WSA-ENLIL are invoked to provide predictions or post-event assessments of plasma speed, interplanetary-field polarity, and the time of arrival at a certain location of a CME-initiated interplanetary shock (*e.g.* Mays *et al.*, 2015; Wold *et al.*, 2018; Riley *et al.*, 2018).

One of the main limitations of ENLIL cone-model simulations is the lack of the internal (driver) magnetic field of the ICME. Versions with flux-rope or spheromak CME ejecta inserted at the inner boundary are in development (Odstrcil, Savani, and Rouillard, 2018). Including the internal magnetic field is essential to forecasting the geomagnetic potential of CMEs and capturing the physics of ICME evolution more accurately. Other heliospheric MHD codes for space-weather forecasting and research support are under development especially in Europe – the European heliospheric forecasting information asset (EUHFORIA: Pomoell and Poedts, 2018; Poedts, 2019; Verbeke, Pomoell, and Poedts, 2019) – and in Japan – the Space-weather-forecast-Usable System Anchored by Numerical Operations and Observations–CME (SUSANOO: Shiota and Kataoka, 2016). Similar to ENLIL, a major advantage of these numerical simulations starting at or above 0.1 AU is that they are inexpensive to run for multiple realizations of events in 3D. They are thus frequently used to complement remote observations in retrospective event analyses or in forecasting an observed CME's effects at 1 AU. The information they can provide includes the longitudinal extent of the ICMEs, the magnetic connectivity of particular heliospheric locations to their shocks, and the related *in-situ* plasma parameters. They moreover give important insights into the nature and effects of their solar-wind interactions in transit (*e.g.* Prise *et al.*, 2015; Winslow *et al.*, 2016; Witasse *et al.*, 2017; Kilpua *et al.*, 2019). There are now ongoing efforts to make more routine simulations of complex CME/ICME simulations that are initiated at the solar surface for both research support and eventually space-weather forecasting (Borvikov *et al.*, 2017; Jin *et al.*, 2017). However, unraveling the detailed physics and phenomena of the CME–ICME relationship and its radial evolution, in realistic contexts, demands further developments of more physically complete simulations.

While still not in the regular-use domain, these state-of-the-art numerical simulations have been useful for retrospectively analyzing real cases where relatively complete observations and measurements related to CMEs and their evolution into ICMEs are available. Synthetic images derived from the simulations are often used to understand remote coronal and heliospheric observations (Lugaz *et al.*, 2008, 2009; Manchester *et al.*, 2008; Odstrcil and Pizzo, 2009; Shen *et al.*, 2018; Jin *et al.*, 2017). For example, they have been applied to the interpretation of the EUV waves (Chen, Fang, and Shibata, 2005; Delannée *et al.*, 2008; Cohen *et al.*, 2009; Downs *et al.*, 2011). Vourlidas *et al.* (2013) used such simulations to analyze the nature of CMEs in terms of the presence/absence of a twisted magnetic-flux rope in white-light images. Lynch *et al.* (2010, 2016) and Lynch and Edmonson (2013) were able to reproduce the appearance of eruptions originating in helmet streamers and pseudostreamers. Lynch and Edmonson (2013) and Török *et al.* (2018) created detailed physical descriptions of the pre-existing magnetic topology before eruptions, including the coronal helmet streamers, pseudostreamers, and null points. A particular contribution to our understanding from the improving simulations concerns the eruptions of multiple CMEs from different active regions, referred to as "sympathetic" CMEs, which are ubiquitous during active times of the solar cycle (Török *et al.*, 2011; Lynch and Edmonson, 2013). While calculations at this level of sophistication that include the 1 AU consequences for validation against *in-situ* observations remain a challenge, they are seeing increasing applications. Al-Haddad *et al.* (2019) compared the properties of ICMEs hypothetically observed by multiple spacecraft assuming two different simulated CME magnetic morphologies. They learned that it was difficult to infer the initial coronal structure from the *in-situ* signatures. Reinard, Lynch, and Mulligan (2012) used simulations and *in-situ* measurements to interpret the ion composition within the structures of ICMEs toward better mapping back to their solar origins.

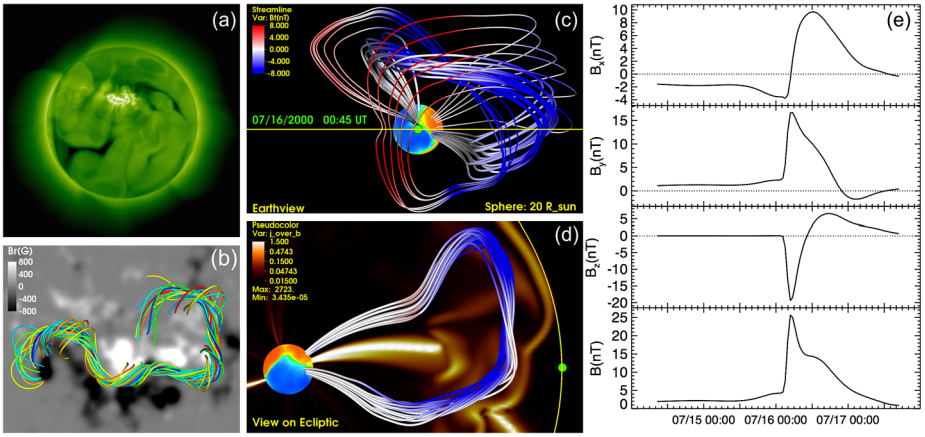

Figure 8 Simulation results of Török *et al.* (2018) (organized from a review by Manchester *et al.*, 2017) illustrating the potential of simulating a CME/ICME event from its solar source to a heliospheric observer site at 1 AU. Such detailed simulations require sufficient observations to both accurately launch the erupting coronal structure in realistic surroundings and have it propagate through realistic solar, wind conditions. (Image reproduced with permission from Manchester *et al.* (2017), copyright by the authors.)

Lastly, simulations, often involving complex initiation mechanisms, are at the center of current efforts to better understand the physical processes that occur during CME propagation into the heliosphere. Manchester *et al.* (2014) followed up on the study of observationally inferred CME erosion using *in-situ* measurements (Ruffenach *et al.*, 2012; Lavraud *et al.*, 2014) with a Sun-to-1 AU numerical simulation. They found that the erosion due to magnetic reconnection between the ICME and the interplanetary magnetic fields occurred, but was relatively limited. However, there was extensive magnetic-field reconfiguration as the simulated CME/ICME propagated from the Sun to 1 AU (see also Manchester, van der Holst, and Lavraud, 2014). A similar, complex reconfiguration and distortion of the original coronal flux rope was evident in another Sun-to-Earth simulation with a different code and initiation mechanism (Török *et al.*, 2018). That study, moreover, found that complexity could result in highly different model-based magnetic-field temporal profiles determined for locations only 10 – 15° apart, as suggested by the earlier work of Riley *et al.* (2004). A recent analysis of multi-spacecraft measurements separated by $\approx 0.7°$ confirmed that significant differences of the magnetic fields of ICMEs at these separations are possible (Lugaz *et al.*, 2018). The complex nature of the magnetic field inside CMEs, and its implications for ICMEs, was similarly highlighted in a simulation by Savani *et al.* (2013). Simulations are also particularly useful for investigating the physical processes occurring during CME–CME or CME–ambient structure interactions. As examples, simulations have been run to understand the evolution of ICME shocks propagating inside previous eruptions (Schmidt and Cargill, 2004; Lugaz, Manchester, and Gombosi, 2005; Mao *et al.*, 2017), super-elastic collisions between CMEs (Shen *et al.*, 2012, 2013), and the previously discussed magnetic reconnection expected to occur between erupted structures and their surroundings, as well as within the structures themselves (Lionello *et al.*, 2013; Lugaz *et al.*, 2013).

The ultimate goal of CME/ICME simulations is the greater physical understanding of their variety of origins and outcomes. A vision for the future continues to be the ability to simulate the full, coupled space-weather chain of events based on observations of the Sun and *in-situ* validations (see Figure 8). However, earlier success, and the insights it brings,

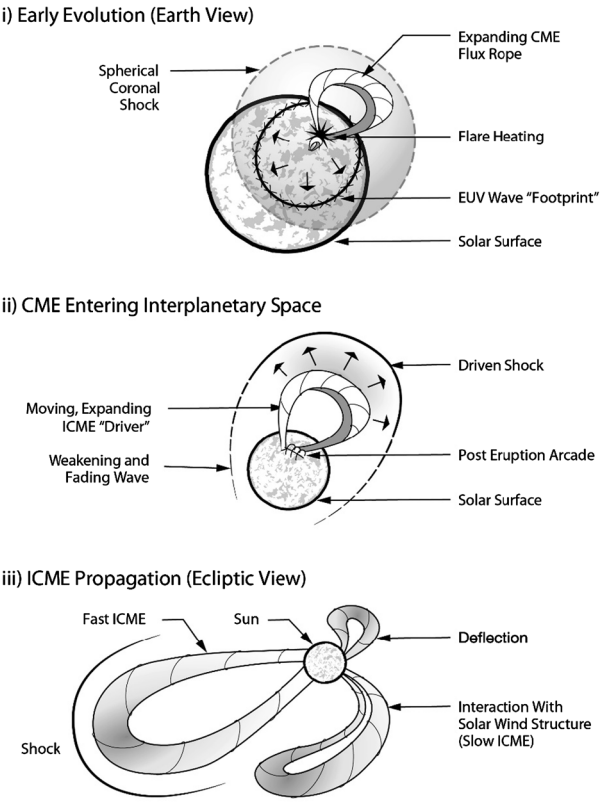

Figure 9 Sketch showing some of the updates to our picture of ICMEs as described in this overview, including **i**) the spherical shock associated with the early evolution of major CMEs, including the EUV wave that may be a signature of its low coronal intersection; **ii**) the development of the longer-lived driven shock that may at first strengthen with distance from the Sun, and can be detected *in situ* at and beyond 1 AU; **iii**) the various behaviors that are inferred as different ICMEs evolve, including deflections from the initial CME direction near the Sun, changes associated with subsequent solar-wind structure interactions, and classical nearly self-similar expansion. Additional effects not shown here include rotation, erosion, and interactions (and sometimes mergers) with other ICMEs. Which of these occurs depends both on the properties and location of the ejecta, and the conditions in the ambient medium (corona and solar wind).

is likely to come by focusing on the simplest cases first. Perhaps these involve the isolated eruption of large filament channels associated with decayed active regions. While simulations have successfully reproduced the images of a slow, streamer-blowout CME (Lynch *et al.*, 2016), the realistic propagation/evolution of the structure and its solar-wind interaction *en route* to ≈ 1 AU represents a necessary and achievable next step. The current solar minimum should provide additional simulation-worthy cases, especially of the relatively simple streamer blowout CMEs (*e.g.* Vourlidas and Webb, 2018) that may dominate space-weather conditions over the next three years or so.

6. Inner Heliosphere ICME Evolution: Future Prospects

This overview has only touched on the substantial progress in observations and physical understanding of ICMEs achieved in the last decade. Going forward, the outstanding issues and challenges include determining how the evolution of the *Heliophysics System Observatory* will affect our ability to both reconstruct their Sun-to-1 AU behavior and interpret it. SOHO, STEREO, and now SDO observations continue to be regularly used in conjunction with *in-situ* observations as well as global coronal and heliospheric models to determine which solar and interplanetary events are related, and how they are related. An updated sketch of what an ICME includes, as we currently understand it, is shown in Figure 9. The flux-rope-like driver continues to be central to the process, although its origin is now considered, and scrutinized, in much more detail. Figure 9 includes some key details described in

this brief overview that are missing in Figure 1. These include near-Sun evolution involving an early-phase pressure wave or shock that gives way to the driven shock observed in the heliosphere. Expansion is regarded as an essential process in the ICME evolution, with its contribution to shock formation being case-dependent. Self-similar expansion of the coronal entity is no longer regarded as the norm for interpreting ICMEs. Realistic, 3D models of the originating coronal and solar-wind structures push the state of the art in describing ambient conditions, while various descriptions of injected coronal structures – with increasingly detailed attributes – are being tested. The heliophysics community is at the threshold of being able to routinely fit models of CME structures seen in multi-perspective coronal images that become the ICMEs observed at 1 AU, with the realistic influences of the ambient medium the next frontier. The availability of both the L_1 assets and STEREO data with their well-separated (relative to L_1) perspective continues to both motivate this work and provide the observational basis for its validation. The ultimate goal is sufficient understanding to reproduce, with physics-based global models, the observed multipoint ICME attributes based on solar observations.

Although MESSENGER and VEX are no longer in operation, MAVEN's ongoing measurements of plasma, field, and energetic particles at Mars, and MSL's RAD surface-radiation measurements, rely on SOHO/ACE/*Wind* (and eventually IMAP) L_1 and STEREO observations for understanding the local effects of solar activity and ICME impacts. Future opportunities include various alignments (radial and Parker Spiral) of Earth, Mars, and STEREO-A for *in-situ* studies, and quadrature configurations providing imaging of CMEs destined for various targets. These will also help set the heliospheric context for upcoming *BepiColombo* observations, and they will provide similar support for Venus flybys of the *Parker Solar Probe* and *Solar Orbiter* missions. Finally, STEREO-A is in a position to test the L_5 concept of Earth space-weather monitoring (*e.g.* Lavraud *et al.*, 2016), including ICME evolution from Sun to Earth, on which we may someday all depend. The heliospheric imagers onboard STEREO have allowed us to image ICMEs directly as they impact spacecraft in the inner heliosphere (MESSENGER, VEX, ACE/*Wind*) that make *in-situ* measurements. MESSENGER highlighted, 30 years after *Helios*, the importance of having *in-situ* measurements of ICMEs in the inner heliosphere. The *Parker Solar Probe* is taking *in-situ* measurements while they are still in the upper corona and visible in the LASCO-C3 field-of-view. Its observations will further advance our understanding by providing a more pristine view of "young" ICMEs only a few hours after their initiation. These measurements, especially those obtained in conjunction with other spacecraft, will further advance our understanding of the origins of the magnetic ejecta, the formation of the shock waves, and the development of the ICME sheaths. In addition to providing a second near-Sun probe, during its extended mission, *Solar Orbiter* will provide the first comprehensive images of ICMEs from a vantage point away from the Ecliptic, allowing further investigations of ICME radial evolution including deflections and interactions. Finally, with the increasing uses of magnetographs on missions, including *Solar Orbiter*, the next major leaps in real event simulations are imminent.

Acknowledgements J.G. Luhmann was supported for her role in this effort by NASA Grant NNX15AG09G to the University of California, Berkeley for the STEREO-IMPACT investigation. L.K. Jian is supported by NASA's Science Mission Directorate as part of the STEREO project, NASA's Living with a Star and Heliophysics Supporting Research programs. N. Gopalswamy is supported by NASA's LWS program. N. Lugaz is supported by NASA grant NNX15AB87G. The authors are also grateful to the reviewer for their careful review and suggestions.

Disclosure of Potential Conflicts of Interest The authors declare that they have no conflicts of interest.

References

Al-Haddad, N., Nieves-Chinchilla, T., Savani, N.P., Möstl, C., Marubashi, K., Hidalgo, M.A., Roussev, I.I., Poedts, S., Farrugia, C.J.: 2013, Magnetic field configuration models and reconstruction methods for interplanetary coronal mass ejections. *Solar Phys.* **284**, 129. DOI. ADS.

Al-Haddad, N., Poedts, S., Roussev, I., Farrugia, C.J., Yu, W., Lugaz, N.: 2019, The magnetic morphology of magnetic clouds: multi-spacecraft investigation of twisted and writhed coronal mass ejections. *Astrophys. J.* **870**, 100. DOI.

Arge, C.N., Pizzo, V.J.: 2000, Improvement in the prediction of solar wind conditions using near-real time solar magnetic field updates. *J. Geophys. Res.* **105**, 10469.

Attrill, G.D.R., Harra, L.K., van Driel-Gesztelyi, L., Démoulin, P.: 2007, Coronal "wave": magnetic footprint of a coronal mass ejection? *Astrophys. J. Lett.* **656**, L101.

Bain, H.M., Mays, M.L., Luhmann, J.G., Li, Y., Jian, L.K., Odstrcil, D.: 2016, Shock connectivity in the August 2010 and July 2012 solar energetic particle events inferred from observations and ENLIL modeling. *Astrophys. J.* **825**, 1. DOI.

Baker, D.N., Poh, G., Odstrcil, D., Arge, C.N., Benna, M., Johnson, C.L., *et al.*: 2013, Solar wind forcing at Mercury: WSA-ENLIL model results. *J. Geophys. Res.* **118**, 45. DOI.

Blanco-Cano, X., Kajdic, P., Aguilar-Rodríguez, E., Russell, C.T., Jian, L.K., Luhmann, J.G.: 2016, Interplanetary shocks and foreshocks observed by STEREO during 2007-2010. *J. Geophys. Res.* **121**, 992. DOI.

Borovsky, J.E., Denton, M.H.: 2006, Differences between CME-driven storms and CIR-driven storms. *J. Geophys. Res.* **111**, A07S08. DOI.

Borvikov, D., Sokolov, I.V., Manchester, W.B., Jin, M., Gombosi, T.: 2017, Eruptive event generator based on the Gibson-low magnetic configuration. *J. Geophys. Res.* **122**, 7974.

Bougeret, J.-L., Kaiser, M.L., Kellogg, P.J., Manning, R., Goetz, K., Monson, S.J., Monge, N., Friel, L., Meetre, C.A., Perche, C., Sitruk, L., Hoang, S.: 1995, WAVES: the radio and plasma wave investigation on the wind spacecraft. *Space Sci. Rev.* **71**, 231.

Burlaga, L.F., Sittler, E., Mariani, F., Schwenn, R.: 1981, Magnetic loop behind an interplanetary shock: Voyager, Helios and IMP-8 observations. *J. Geophys. Res.* **86**, 6673.

Burns, A.G., Solomon, S.C., Wang, W., Killeen, T.L.: 2007, The ionospheric and thermospheric response to CMEs: challenges and successes. *J. Atmos. Solar-Terr. Phys.* **69**, 77. DOI.

Cane, H.V., Sheeley, N.R. Jr., Howard, R.A.: 1987, Energetic interplanetary shocks, radio emission, and coronal mass ejections. *J. Geophys. Res.* **92**, 9869.

Cane, H.V., Stone, R.G.: 1984, Type II solar radio bursts, interplanetary shocks, and energetic particle events. *Astrophys. J.* **282**, 339.

Chen, P.F., Fang, C., Shibata, K.: 2005, A full view of EIT waves. *Astrophys. J.* **622**, 1202.

Chen, J., Howard, R.A., Brueckner, G.E., Santoro, R., Krall, J., Paswaters, S.E., St. Cyr, O.C., Schwenn, R., Lamy, P., Simnett, G.M.: 1997, Evidence of an erupting magnetic flux rope: LASCO coronal mass ejection of 1997 April 13. *Astrophys. J. Lett.* **490**, L191. DOI.

Chi, Y., Shen, C., Wang, Y.: 2016, Statistical study of the interplanetary coronal mass ejections from 1995 to 2015. *Solar Phys.* **291**, 2419. DOI. ADS.

Cho, K.-S., Park, S.-H., Marubashi, K., Gopalswamy, N., Akiyama, S., Yashiro, S., Kim, R.-S., Lim, E.-K.: 2013, Comparison of helicity signs in interplanetary CMEs and their solar source regions. *Solar Phys.* **284**, 105. DOI. ADS.

Cohen, C.M.S.: 2006, Observations of energetic storm particles: an overview, in solar eruptions and energetic particles. In: Gopalswamy, N., Mewaldt, R., Torsti, J. (eds.) *Geophys. Monogr. Ser.* **165**, 275. DOI.

Cohen, O., Attrill, G.D., Manchester, W.B., Wills-Davey, M.J.: 2009, Numerical simulation of an EUV coronal wave based on the 2009 February 13 CME event observed by STEREO. *Astrophys. J.* **705**, 587.

Conner, H.K., Zesta, E., Fedrizzi, M., Shi, Y., Raeder, J., Codrescu, M.V., Fuller-Rowell, T.J.: 2016, Modeling the ionosphere-thermosphere response to a geomagnetic storm using physics-based magnetospheric energy input: OpenGGCM-CTIM results. *J. Space Weather Space Clim.* **6**, A25. DOI.

Cremades, H.: 2018, Pursuing forecasts of the behavior and arrival of coronal mass ejections through modeling and observations. In: Foullon, C., Malandraki, O. (eds.) *Space Weather of the Heliosphere: Processes and Forecasts*, *Proc. Inter. Astron. Union S335* **13**, 58. DOI.

Cremades, H., Iglesias, F.A., St. Cyr, O.C., Xie, H., Kaiser, M.L., Gopalswamy, N.: 2015, Low-frequency type-II radio detections and coronagraph data employed to describe and forecast the propagation of 71 CMEs/shocks. *Solar Phys.* **290**, 2455. DOI. ADS.

Dasso, S., Mandrini, C.H., Démoulin, P., Luoni, M.L.: 2006, A new model-independent method to compute magnetic helicity in magnetic clouds. *Astron. Astrophys.* **455**, 349. DOI.

Dasso, S., Nakwacki, M.S., Démoulin, P., Mandrini, C.H.: 2007, Progressive transformation of a flux rope to an ICME. Comparative analysis using the direct and fitted expansion methods. *Solar Phys.* **284**, 115. DOI.

Delannée, C., Török, T., Aulanier, G., Hochedez, J.F.: 2008, A new model for propagating parts of EIT waves: a current shell in a CME. *Solar Phys.* **247**, 123. DOI. ADS.

Ding, L.-G., Wang, Z.-W., Feng, L., Li, G., Jiang, Y.: 2019, Is the enhancement of type II radio bursts during CME interactions related to the associated solar energetic particle event? *Res. Astron. Astrophys.* **19**, 5.

Downs, C., Roussev, I.I., van der Holst, B., Lugaz, N., Sokolov, I.V., Gombosi, T.I.: 2011, Studying extreme ultraviolet wave transients with a digital laboratory: direct comparison of extreme ultraviolet wave observations to global magnetohydrodynamic simulations. *Astrophys. J.* **728**, 2.

Fan, Y., Gibson, S.E.: 2007, Onset of coronal mass ejections due to loss of confinement of coronal flux ropes. *Astrophys. J.* **668**, 1232.

Farrugia, C.J., Berdichevsky, D.B., Möstl, C., Galvin, A.B., Leitner, M., Popecki, M.A., Simunac, K.D.C., Opitz, A., Lavraud, B., Ogilvie, K.W., Veronig, A.M., Temmer, M., Luhmann, J.G., Sauvaud, J.A.: 2011, Multiple, distant (40°) in situ observations of a magnetic cloud and a corotating interaction region complex. *J. Atmos. Solar-Terr. Phys.* **73**, 1254. DOI.

Fisher, R.R., Munro, R.H.: 1984, Coronal transient geometry. I. The flare-associated event of 1981 March 25. *Astrophys. J.* **280**, 428.

Forbes, T.G.: 2000, A review on the genesis of coronal mass ejections. *J. Geophys. Res.* **105**, 23153.

Fox, N.J., Velli, M.C., Bale, S.D., Decker, R., Driesman, A., Howard, R.A., Kasper, J.C., Kinnison, J., Kusterer, M., Lario, D., Lockwood, M.K., McComas, D.J., Raouafi, N.E., Szabo, A.: 2016, The solar probe plus mission: humanity's first visit to our star. *Space Sci. Rev.* **204**, 7. DOI.

Gonzalez, W.D., Tsurutani, B.T.: 1987, Criteria of interplanetary parameters causing intense magnetic storms (Dst < 100 nT). *Planet. Space Sci.* **35**, 1101.

Good, S.W., Forsyth, R.J.: 2016, Interplanetary coronal mass ejections observed by MESSENGER and Venus Express. *Solar Phys.* **291**, 239. DOI. ADS.

Good, S.W., Forsyth, R.J., Raines, J.M., Gershman, D.J., Slavin, J.A., Zurbuchen, T.H.: 2015, Radial evolution of a magnetic cloud: MESSENGER, STEREO, and Venus Express observations. *Astrophys. J.* **807**, 177.

Good, S.W., Kilpua, E.K.J., LaMoury, A.T., Forsyth, R.J., Eastwood, J.P., Möstl, C.: 2019, Self-similarity of ICME flux ropes: observations by radially aligned spacecraft in the inner heliosphere. *J. Geophys. Res.* **124**, 4960. DOI.

Gopalswamy, N.: 2006a, Properties of interplanetary coronal mass ejections. *Space Sci. Rev.* **124**, 145.

Gopalswamy, N.: 2006b, Coronal mass ejections and type II radio bursts. In: Gopalswamy, N., Mewaldt, R., Torsti, J. (eds.) *Solar Eruptions and Energetic Particles*, *Geophys. Monogr. Ser.* **165**, Am. Geophys. Union, Washington, 207.

Gopalswamy, N.: 2008, Solar connections of geoeffective magnetic structures. *J. Atmos. Solar-Terr. Phys.* **70**, 2078.

Gopalswamy, N.: 2011, Coronal mass ejections and solar radio emissions. In: Rucker, H.O., Kurth, W.S., Louarn, P., Fischer, G. (eds.) *Planetary Radio Emissions VII, Proc. 7th Internat. Workshop on Planetary, Solar Heliospheric Radio Emissions*, Austrian Acad. Sci. Press, Vienna, 325.

Gopalswamy, N.: 2016, History and development of coronal mass ejections as a key player in solar terrestrial relationship. *Geosci. Lett.* **3**, 8.

Gopalswamy, N., Tsurutani, B., Yan, Y.: 2015, Short-term variability of the Sun-Earth system: an overview of progress made during the CAWSES-II period. *Prog. Earth Planet. Sci.* **2**, 13.

Gopalswamy, N., Yashiro, S.: 2011, The strength and radial profile of the coronal magnetic field from the standoff distance of a coronal mass ejection-driven shock. *Astrophys. J. Lett.* **736**, L17.

Gopalswamy, N., Yashiro, S., Kaiser, M.L., Howard, R.A., Bougeret, J.-L.: 2001a, Radio signatures of coronal mass ejection interaction: coronal mass ejection cannibalism? *Astrophys. J. Lett.* **548**, L91.

Gopalswamy, N., Lara, A., Yashiro, S., Kaiser, M.L., Howard, R.A.: 2001b, Predicting the 1-AU arrival times of coronal mass ejections. *J. Geophys. Res.* **106**, 29207.

Gopalswamy, N., Lara, A., Kaiser, M.L., Bougeret, J.-L.: 2001c, Near-Sun and near-Earth manifestations of solar eruptions. *J. Geophys. Res.* **106**, 25261.

Gopalswamy, N., Yashiro, S., Michalek, G., Kaiser, M.L., Howard, R.A., Reames, D.V., Leske, R., von Rosenvinge, T.: 2002, Interacting coronal mass ejections and solar energetic particles. *Astrophys. J. Lett.* **572**, L103.

Gopalswamy, N., Yashiro, S., Krucker, S., Stenborg, G., Howard, R.A.: 2004, Intensity variation of large solar energetic particle events associated with coronal mass ejections. *J. Geophys. Res.* **109**, A12105.

Gopalswamy, N., Aguilar-Rodriguez, E., Yashiro, S., Nunes, S., Kaiser, M.L., Howard, R.A.: 2005, Type II radio bursts and energetic solar eruptions. *J. Geophys. Res.* **110**, A12S07.
Gopalswamy, N., Dal Lago, A., Yashiro, S., Akiyama, S.: 2009a, The expansion and radial speeds of coronal mass ejections. *Cent. Eur. Astrophys. Bull.* **33**, 115.
Gopalswamy, N., Mäkelä, P., Xie, H., Akiyama, S., Yashiro, S.: 2009b, CME interactions with coronal holes and their interplanetary consequences. *J. Geophys. Res.* **114**, 0A22G.
Gopalswamy, N., Thompson, W.T., Davila, J.M., Kaiser, M.L., Yashiro, S., Mäkelä, P., Michalek, G., Bougeret, J.-L., Howard, R.A.: 2009c, Relation between type II bursts and CMEs inferred from STEREO observations. *Solar Phys.* **259**, 227. DOI. ADS.
Gopalswamy, N., Xie, H., Mäkelä, P., Akiyama, S., Yashiro, S., Kaiser, M.L., Howard, R.A., Bougeret, J.-L.: 2010, Interplanetary shocks lacking type II radio bursts. *Astrophys. J.* **710**, 1111.
Gopalswamy, N., Nitta, N., Akiyama, S., Mäkelä, P., Yashiro, S.: 2012a, Coronal magnetic field measurement from EUV images made by the Solar Dynamics Observatory. *Astrophys. J.* **744**, 72.
Gopalswamy, N., Mäkelä, P., Akiyama, S., Yashiro, S., Xie, H., MacDowall, R.J., Kaiser, M.L.: 2012b, Radio-loud CMEs from the disk center lacking shocks at 1 AU. *J. Geophys. Res.* **117**, 8106.
Gopalswamy, N., Xie, H., Yashiro, S., Akiyama, S., Mäkelä, P., Usoskin, I.G.: 2012c, Properties of ground level enhancement events and the associated solar eruptions during solar cycle 23. *Space Sci. Rev.* **171**, 23.
Gopalswamy, N., Mäkelä, P., Akiyama, S., Xie, H., Yashiro, S., Reinard, A.A.: 2013a, The solar connection of enhanced heavy ion charge states in the interplanetary medium: implications for the flux-rope structure of CMEs. *Solar Phys.* **284**, 17. DOI. ADS.
Gopalswamy, N., Nieves-Chinchilla, T., Hidalgo, M., Zhang, J., Riley, P., van Driel-Gesztelyi, L., Mandrini, C.H.: 2013b, Preface. *Solar Phys.* **284**, 1. DOI. ADS.
Gopalswamy, N., Mäkelä, P., Xie, H., Yashiro, S.: 2013c, Testing the empirical shock arrival model using quadrature observations. *Space Weather* **11**, 661.
Gopalswamy, N., Xie, H., Mäkelä, P., Yashiro, S., Akiyama, S., Uddin, W., Srivastava, A.K., Joshi, N.C., Chandra, R., Manoharan, P.K., Mahalakshmi, K., Dwivedi, V.C., Jain, R., Awasthi, A.K., Nitta, N.V., Aschwanden, M.J., Choudhary, D.P.: 2013d, Height of shock formation in the solar corona inferred from observations of type II radio bursts and coronal mass ejections. *Adv. Space Res.* **51**, 1981.
Gopalswamy, N., Xie, H., Akiyama, S., Yashiro, S., Usoskin, I.G., Davila, J.M.: 2013e, The first ground level enhancement event of solar cycle 24: direct observation of shock formation and particle release heights. *Astrophys. J. Lett.* **765**, L30.
Gopalswamy, N., Xie, H., Akiyama, S., Mäkelä, P.A., Yashiro, S.: 2014a, Major solar eruptions and high-energy particle events during solar cycle 24. *Earth Planets Space* **66**, 104.
Gopalswamy, N., Akiyama, S., Yashiro, S., Xie, H., Mäkelä, P., Michalek, G.: 2014b, Anomalous expansion of coronal mass ejections during solar cycle 24 and its space weather implications. *Geophys. Res. Lett.* **41**, 2673.
Gopalswamy, N., Yashiro, S., Xie, H., Akiyama, S., Mäkelä, P.: 2015a, Properties and geoeffectiveness of magnetic clouds during solar cycles 23 and 24. *J. Geophys. Res.* **120**, 9221.
Gopalswamy, N., Mäkelä, P., Akiyama, S., Yashiro, S., Thakur, N.: 2015b, CMEs during the two activity peaks in cycle 24 and their space weather consequences. *Sun Geosph.* **10**, 111.
Gopalswamy, N., Mäkelä, P., Akiyama, S., Yashiro, S., Xie, H., Thakur, N., Kahler, S.W.: 2015c, Large solar energetic particle events associated with filament eruptions outside of active regions. *Astrophys. J.* **806**, 8.
Gopalswamy, N., Yashiro, S., Thakur, N., Mäkelä, P., Xie, H., Akiyama, S.: 2016, The 2012 July 23 backside eruption: an extreme energetic particle event? *Astrophys. J.* **833**, 216.
Gopalswamy, N., Yashiro, S., Akiyama, S., Xie, H.: 2017a, Estimation of reconnection flux using post-eruption arcades and its relevance to magnetic clouds at 1 AU. *Solar Phys.* **292**, 65. DOI. ADS.
Gopalswamy, N., Mäkelä, P., Yashiro, S., Thakur, N., Akiyama, S., Xie, H.: 2017b, A hierarchical relationship between the fluence spectra and CME kinematics in large solar energetic particle events: a radio perspective. *J. Phys.* **CS-900**, 012009.
Gopalswamy, N., Akiyama, S., Yashiro, S., Xie, H.: 2018a, Coronal flux ropes and their interplanetary counterparts. *J. Atmos. Solar-Terr. Phys.* **180**, 35.
Gopalswamy, N., Akiyama, S., Yashiro, S., Xie, H.: 2018b, A new technique to provide realistic input to CME forecasting models. In: Foullon, C., Malandraki, O. (eds.) *Space Weather of the Heliosphere: Processes and Forecasts*, *Proc. Inter. Astron. Union S335* **13**, 258. DOI.
Gopalswamy, N., Yashiro, S., Mäkelä, P., Xie, H., Akiyama, S., Monstein, C.: 2018c, Extreme kinematics of the 2017 September 10 solar eruption and the spectral characteristics of the associated energetic particles. *Astrophys. J. Lett.* **863**, L39.
Gopalswamy, N., Mäkelä, P., Akiyama, S., Yashiro, S., Xie, H., Thakur, N.: 2018d, Sun-to-Earth propagation of the 2015 June 21 coronal mass ejection revealed by optical, EUV, and radio observations. *J. Atmos. Solar-Terr. Phys.* **179**, 225.

Gosling, J.T.: 1993, The solar flare myth. *J. Geophys. Res.* **98**, 18937.
Green, L.M., Török, T., Vršnak, B., Manchester, W., Veronig, A.: 2018, The origin and early evolution of solar eruptions. *Space Sci. Rev.* **214**, 46. DOI.
Gruesbeck, J.R., Lepri, S.T., Zurbuchen, T.H.: 2012, Two-plasma model for low charge state interplanetary coronal mass ejection observations. *Astrophys. J.* **760**, 141.
Harrison, R.A., Davies, J.A., Möstl, C., Liu, Y., Temmer, M., Bisi, M.M., Eastwood, J.P., de Koning C.A., Nitta, A., Rollett, T.: 2012, An analysis of the origin and propagation of the multiple coronal mass ejections of 2010 August 1. *Astrophys. J.* **750**, 45. DOI.
Harrison, R.A., Davies, J.A., Barnes, D., Byrne, J.P., Perry, C.H., Bothmer, V., Eastwood, J.P., Gallagher, P.T., Kilpua, E.K.J., Möstl, C., Rodriguez, L., Rouillard, A.P., Odstrcil, D.: 2018, CMEs in the heliosphere: I. A statistical analysis of the observational properties of CMEs detected in the heliosphere from 2007 to 2017 by STEREO/HI-1. *Solar Phys.* **293**, 77. DOI. ADS.
He, W., Liu, Y.D., Hu, H., Wang, R., Zhao, X.: 2018, A stealth CME bracketed between slow and fast wind producing unexpected geoeffectiveness. *Astrophys. J.* **860**, 78.
Hess, P., Colaninno, R.C.: 2017, Comparing automatic CME detections in multiple LASCO and SECCHI catalogs. *Astrophys. J.* **836**, 134.
Hess, P., Zhang, J.: 2014, Stereoscopic study of the kinematic evolution of a coronal mass ejection and its driven shock from the Sun to the Earth and the prediction of their arrival times. *Astrophys. J.* **792**, 49.
Howard, T.A., Simnett, G.: 2008, Interplanetary coronal mass ejections that are undetected by solar coronagraphs. *J. Geophys. Res.* **113**, A08102. DOI.
Hu, Q., Qiu, J., Dasgupta, B., Khare, A., Webb, G.M.: 2014, Structures of interplanetary magnetic flux ropes and comparison with their solar sources. *Astrophys. J.* **793**, 2014.
Isavnin, A.: 2016, FRiED: a novel three-dimensional model of coronal mass ejections. *Astrophys. J.* **833**, 267.
Isavnin, A., Vourlidas, A., Kilpua, E.K.J.: 2013, Three-dimensional evolution of erupted flux-rope CMEs from the Sun (2–20 R.) to 1 AU. *Solar Phys.* **284**, 203. DOI. ADS.
Isavnin, A., Vourlidas, A., Kilpua, E.K.J.: 2014, Three-dimensional evolution of flux-rope CMEs and its relation to the local orientation of the heliospheric current sheet. *Solar Phys.* **289**, 2141. DOI. ADS.
Janvier, M., Démoulin, P., Dasso, S.: 2014, Mean shape of interplanetary shocks deduced from in situ observations and its relation with interplanetary CMEs. *Astron. Astrophys.* **565**, A99. DOI.
Janvier, M., Winslow, R.M., Good, S., Bonhomme, E., Démoulin, P., Dasso, S., Möstl, C., Lugaz, N., Amerstorfer, T., Soubrié, E., Boakes, P.D.: 2019, Generic magnetic field intensity profiles of interplanetary coronal mass ejecta at Mercury, Venus and Earth from superposed epoch analysis. *J. Geophys. Res.* **124**, 812.
Jian, L.K., Russell, C.T., Luhmann, J.G.: 2011, Comparing solar minimum 23/24 with historical solar wind records at 1 AU. *Solar Phys.* **274**, 321. DOI. ADS.
Jian, L., Russell, C.T., Luhmann, J.G., Skoug, R.M.: 2006, Properties of interplanetary coronal mass ejections at one AU during 1995-2004. *Solar Phys.* **239**, 393. DOI. ADS.
Jian, L.K., Russell, C.T., Luhmann, J.G., Skoug, R.M., Steinberg, J.T.: 2008a, Stream interactions and interplanetary coronal mass ejections at 0.72 AU. *Solar Phys.* **249**, 85. DOI. ADS.
Jian, L.K., Russell, C.T., Luhmann, J.G., Skoug, R.M., Steinberg, J.T.: 2008b, Stream interactions and interplanetary coronal mass ejections at 5.3 AU near the solar ecliptic plane. *Solar Phys.* **250**, 375. DOI. ADS.
Jian, L., Russell, C.T., Luhmann, J.G., Skoug, R.M.: 2008c, Evolution of solar wind structures from 0.72 to 1 AU. *Adv. Space Res.* **41**, 259. DOI.
Jian, L.K., Russell, C.T., Luhmann, J.G., Galvin, A.B.: 2018d, STEREO observations of interplanetary coronal mass ejections in 2007-2016. *Astrophys. J.* **885**, 114.
Jin, M., Manchester, W.B., van der Holst, B., Sokolov, I., Tóth, G., Vourlidas, A.: 2017, Chromosphere to 1 au simulation of the 2011 March 7th event: a comprehensive study of coronal mass ejection propagation. *Astrophys. J.* **834**, 172.
Kahler, S.W.: 2001, The correlation between solar energetic particle peak intensities and speeds of coronal mass ejections: effects of ambient particle intensities and energy spectra. *J. Geophys. Res.* **106**, 20947.
Kay, C., Opher, M.: 2015, The heliocentric distance where the deflections and rotations of solar coronal mass ejections occur. *Astrophys. J. Lett.* **811**, L36.
Kay, C., Opher, M., Evans, R.M.: 2015, Global trends of CME deflections based on CME and solar parameters. *Astrophys. J.* **805**, 168. DOI.
Kilpua, E., Koskinen, H.E.J., Pulkkinen, T.I.: 2017, Coronal mass ejections and their sheath regions in interplanetary space. *Liv. Rev. Solar Phys.* **14**, 5. DOI.
Kilpua, E.K.J., Lumme, E., Andreeova, K., Isavnin, A., Koskinen, H.E.J.: 2015, Properties and drivers of fast interplanetary shocks near the orbit of the Earth (1995–2013). *J. Geophys. Res.* **120**, 4112. DOI.

Kilpua, E.K.J., Lugaz, N., Mays, M.L., Temmer, M.: 2019, Forecasting the structure and orientation of earth-bound coronal mass ejections. *Space Weather* **17**, 498. DOI.
Kim, R.S., Gopalswamy, N., Cho, K.-S., Moon, Y.J., Yashiro, S.: 2013, Propagation characteristics of CMEs associated with magnetic clouds and ejecta. *Solar Phys.* **284**, 77. DOI. ADS.
Klein, L.W., Burlaga, L.F.: 1982, Interplanetary magnetic clouds at 1 AU. *J. Geophys. Res.* **87**, 613.
Kozarev, K.A., Korreck, K., Lobzin, V.V., Weber, M.A., Schwadron, N.A.: 2011, Off-limb solar coronal wavefronts from SDO/AIA extreme-ultraviolet observations—implications for particle production. *Astrophys. J.* **733**, 25.
Kozarev, K.A., Raymond, J.C., Lobzin, V.V., Hammer, M.: 2015, Properties of a coronal shock wave as a driver of early SEP acceleration. *Astrophys. J.* **799**, 167.
Kwon, R.Y., Vourlidas, A.: 2017, Investigating the wave nature of the outer envelope of halo coronal mass ejections. *Astrophys. J.* **836**, 246.
Kwon, R.Y., Vourlidas, A.: 2018, The density compression ratio of shock fronts associated with coronal mass ejections. *J. Space Weather Space Clim.* **8**, A08.
Kwon, R.-Y., Zhang, J., Olmedo, O.: 2014, New insights into the physical nature of coronal mass ejections and associated shock waves within the framework of the three-dimensional structure. *Astrophys. J.* **794**, 148. DOI.
Kwon, R.Y., Zhang, J., Vourlidas, A.: 2015, Are halo-like solar coronal mass ejections merely a matter of geometric projection effects? *Astrophys. J. Lett.* **799**, L29.
Lai, H.R., Russell, C.T., Jian, L.K., Blanco-Cano, X., Anderson, B.J., Luhmann, J.G., Wennmacher, A.: 2012, The radial evolution of interplanetary shocks in the inner heliosphere: observations by helios, MESSENGER, and STEREO. *Solar Phys.* **278**, 421. DOI. ADS.
Lario, D., Aran, A., Gómez-Herrero, R., Dresing, N., Heber, B., Ho, G.C., Decker, R.B., Roelof, E.C.: 2013, Longitudinal and radial dependence of solar energetic particle peak intensities: STEREO, ACE, SOHO, GOES, and MESSENGER observations. *Astrophys. J.* **767**, 41. DOI.
Lario, D., Raouafi, N.E., Kwon, R.-Y., Xhang, J., Gómez-Herrero, R., Dresing, N., Riley, P.: 2014, The solar energetic particle event on 2013 April 11: an investigation of its solar origin and longitudinal spread. *Astrophys. J.* **797**, 8. DOI.
Lario, D., Kwon, R.-Y., Vourlidas, A., Raouafi, N.E., Haggerty, D.K., Ho, G.C.: 2016, Longitudinal properties of a widespread solar energetic particle event on 2014 February 25: evolution of the associated CME shock. *Astrophys. J.* **819**, 72.
Lario, D., Kwon, R.-Y., Richardson, I.G., Raouafi, N.E., Thompson, B.J.: 2017, The solar energetic particle event of 2010 August 14: connectivity with the solar source inferred from multiple spacecraft observations and modeling. *Astrophys. J.* **838**, 51.
Lavraud, B., Ruffenach, A., Rouillard, A.P., Kajdic, P., Manchester, W.B., Lugaz, N.: 2014, Geo-effectiveness and radial dependence of magnetic cloud erosion by magnetic reconnection. *J. Geophys. Res.* **119**, 26.
Lavraud, B., Liu, Y., Segura, K., He, J., Qin, G., Temmer, M., *et al.*: 2016, A small mission concept to the Sun–Earth Lagrangian L5 point for innovative solar, heliospheric and space weather science. *J. Atmos. Solar-Terr. Phys.* **146**, 171. DOI.
Leblanc, Y., Dulk, G.A., Bougeret, J.-L.: 1998, Tracing the electron density from the corona to 1 au. *Solar Phys.* **183**, 165. DOI. ADS.
Lee, C.O., Hara, T., Halekas, J.S., Thiemann, E., Chamberlin, P., Eparvier, F.: 2017, MAVEN observations of the solar cycle 24 space weather conditions at Mars. *J. Geophys. Res.* **122**, 2768.
Lepping, R.P., Burlaga, L.F., Jones, J.A.: 1990, Magnetic field structure of interplanetary magnetic clouds at 1 AU. *J. Geophys. Res.* **95**, 11957. DOI.
Lepri, S.T., Zurbuchen, T.H.: 2004, Iron charge state distributions as an indicator of hot ICMEs: possible sources and temporal and spatial variations during solar maximum. *J. Geophys. Res.* **109**, A01112.
Lepri, S.T., Zurbuchen, T.H., Fisk, L.A., Richardson, I.G., Cane, H.V., Gloeckler, G.: 2001, Iron charge distribution as an identifier of interplanetary coronal mass ejections. *J. Geophys. Res.* **106**, 29231.
Li, Y., Luhmann, J.G., Lynch, B.J.: 2018, Magnetic clouds: solar cycle dependence, sources, and geomagnetic impacts. *Solar Phys.* **293**, 135. DOI. ADS.
Li, G., Moore, R., Mewaldt, R.A., Zhao, L., Labrador, A.W.: 2012, A twin-CME scenario for ground level enhancement events. *Space Sci. Rev.* **171**, 141.
Li, Y., Luhmann, J.G., Lynch, B.J., Kilpua, E.: 2014, Magnetic clouds and origins in STEREO era. *J. Geophys. Res.* **119**, 3237. DOI.
Liewer, P., Panasenco, O., Vourlidas, A., Colaninno, R.: 2015, Observations and analysis of the non-radial propagation of coronal mass ejections near the Sun. *Solar Phys.* **290**, 3343. DOI. ADS.
Lionello, R., Linker, J.A., Mikic, Z.: 2009, Multispectral emission of the Sun during the first whole Sun month: magnetohydrodynamic simulations. *Astrophys. J.* **690**, 902.
Lionello, R., Downs, C., Linker, J.A., Török, T., Riley, P., Mikic, Z.: 2013, Magnetohydrodynamic simulations of interplanetary coronal mass ejections. *Astrophys. J.* **777**, 76.

Liu, Y., Thernisien, A., Luhmann, J.G., Vourlidas, A., Davies, J.A., Lin, R.P., Bale, S.D.: 2010, Reconstructing coronal mass ejections with coordinated imaging and in situ observations: global structure, kinematics, and implications for space weather forecasting. *Astrophys. J.* **722**, 1762.

Liu, Y.D., Luhmann, J.G., Lugaz, N., Möstl, C., Davies, J.A., Bale, S.D., Lin, R.P.: 2013, On Sun-to-Earth propagation of coronal mass ejections. *Astrophys. J.* **769**, 45.

Liu, Y.D., Yang, Z., Wang, R., Luhmann, J.G., Richardson, J.D., Lugaz, N.: 2014a, Sun-to-Earth characteristics of two coronal mass ejections interacting near 1 AU: formation of a complex ejecta and generation of a two-step geomagnetic storm. *Astrophys. J.* **793**, 41.

Liu, Y.D., Luhmann, J., Kajdič, P., Kilpua, E.K.J., Lugaz, N., Nitta, N.V., *et al.*: 2014b, Observations of an extreme storm in interplanetary space caused by successive coronal mass ejections. *Nat. Comm.* **5**, 3481. DOI.

Liu, Y.D., Hu, H., Wang, R., Yang, Z., Zhu, B., Liu, Y.-A., *et al.*: 2015, Plasma and magnetic field characteristics of solar coronal mass ejections in relation to geomagnetic storm intensity and variability. *Astrophys. J. Lett.* **809**, L34.

Long, D.M., Bloomfield, D.S., Chen, P.F., Downs, C., Gallagher, P.T., Kwon, R.-Y., Vanninathan, K., Veronig, A.M., Vourlidas, A., Vršnak, B., Warmuth, A., Žic, T.: 2017, Understanding the physical nature of coronal "EIT waves". *Solar Phys.* **292**, 7. DOI. ADS.

Lugaz, N., Manchester, W.B., Gombosi, T.I.: 2005, Numerical simulation of the interaction of two coronal mass ejections from Sun to Earth. *Astrophys. J.* **634**, 651.

Lugaz, N., Vourlidas, A., Roussev, I.I., Jacobs, C., Manchester, W.B., Cohen, O.: 2008, The brightness of density structures at large solar elongation angles: what is being observed by STEREO SECCHI? *Astrophys. J. Lett.* **684**, L111.

Lugaz, N., Vourlidas, A., Roussev, I.I., Morgan, H.: 2009, Solar-terrestrial simulation in the STEREO era: the 24-25 January 2007 eruptions. *Solar Phys.* **256**, 269. DOI. ADS.

Lugaz, N., Hernandez-Charpak, J.N., Roussev, I.I., Davis, C.J., Vourlidas, A., Davies, J.A.: 2010, Determining the azimuthal properties of coronal mass ejections from multi-spacecraft remote-sensing observations with STEREO SECCHI. *Astrophys. J.* **715**, 493.

Lugaz, N., Farrugia, C.J., Davies, J.A., Möstl, C., Davis, C.J., Roussev, I.I., Temmer, M.: 2012, The deflection of the two interacting coronal mass ejections of 2010 May 23-24 as revealed by combined in situ measurements and heliospheric imaging. *Astrophys. J.* **759**, 68.

Lugaz, N., Farrugia, C.J., Manchester, W.B., Schwadron, N.A.: 2013, The interaction of two coronal mass ejections: influence of relative orientation. *Astrophys. J.* **778**, 20.

Lugaz, N., Farrugia, C.J., Winslow, R.M., Al-Haddad, N., Kilpua, E.K.J., Riley, P.: 2016, Factors affecting the geoeffectiveness of shocks and sheaths at 1 AU. *J. Geophys. Res.* **121**, 10861.

Lugaz, N., Temmer, M., Wang, Y., Farrugia, C.J.: 2017a, The interaction of successive coronal mass ejections: a review. *Solar Phys.* **292**, 64. DOI. ADS.

Lugaz, N., Farrugia, C.J., Winslow, R.M., Small, C.R., Manion, T., Savani, N.P.: 2017b, Importance of CME radial expansion on the ability of slow CMEs to drive shocks. *Astrophys. J.* **848**, 75.

Lugaz, N., Farrugia, C.J., Winslow, R.M., Al-Haddad, N., Galvin, A.B., Nieves-Chinchilla, T.: 2018, On the spatial coherence of magnetic ejecta: measurements of coronal mass ejections by multiple spacecraft longitudinally separated by 0.01 au. *Astrophys. J. Lett.* **864**, L7.

Lynch, B.J., Edmonson, J.K.: 2013, Sympathetic magnetic breakout coronal mass ejections from pseudostreamers. *Astrophys. J.* **764**, 87.

Lynch, B.J., Li, Y., Thernisien, A.F.R., Robbrecht, E., Fisher, G.H., Luhmann, J.G., Vourlidas, A.: 2010, Sun to 1 AU propagation and evolution of a slow streamer - blowout coronal mass ejection. *J. Geophys. Res.* **115**, 7106.

Lynch, B.J., Masson, S., Li, Y., DeVore, C.R., Luhmann, J.G., Antiochos, S.K., Fisher, G.H.: 2016, A model for stealth coronal mass ejections. *J. Geophys. Res.* **121**, 10677.

Ma, S., Raymond, J.C., Golub, L., Lin, J., Chen, H., Grigis, P., Testa, P., Long, D.: 2011, Observations and interpretation of a low coronal shock wave observed in the EUV by the SDO/AIA. *Astrophys. J.* **738**, 160.

Mäkelä, P., Gopalswamy, N., Akiyama, S., Xie, H., Yashiro, S.: 2011, Energetic storm particle events in coronal mass ejection-driven shocks. *J. Geophys. Res.* **116**, 1801.

Mäkelä, P., Gopalswamy, X.H., Mohamed, A.A., Akiyama, S., Yashiro, S.: 2013, Coronal hole influence on the observed structure of interplanetary CMEs. *Solar Phys.* **284**, 59. DOI.

Mäkelä, P., Gopalswamy, N., Akiyama, S., Xie, H., Yashiro, S.: 2015, Estimating the height of CMEs associated with a major SEP event at the onset of the metric type ii radio burst during solar cycles 23 and 24. *Astrophys. J.* **806**, 13.

Mäkelä, P., Gopalswamy, N., Reiner, M.J., Akiyama, S., Krupar, V.: 2016, Source regions of the Type II radio burst observed during a CME-CME interaction on 2013 May 22. *Astrophys. J.* **827**, 141.

Manchester, W.B., van der Holst, B., Lavraud, B.: 2014, Flux rope evolution in interplanetary coronal mass ejections: the 13 May 2005 event. *Plasma Phys. Control. Fusion* **56**, 064006.
Manchester, W.B., Vourlidas, A., Tóth, G., Lugaz, N., Roussev, I.I., Sokolov, I.V., Gombosi, T.I., De Zeeuw, D.L., Opher, M.: 2008, Three-dimensional MHD simulation of the 2003 October 28 coronal mass ejection: comparison with LASCO coronagraph observations. *Astrophys. J.* **684**, 1448.
Manchester, W.B., Kozyra, J., Lepri, S.T., Lavraud, B.: 2014, Simulation of magnetic cloud erosion during propagation. *J. Geophys. Res.* **119**, 5449.
Manchester, W., Kilpua, E.K.J., Liu, Y.D., Lugaz, N., Riley, P., Török, T., Vrsnak, B.: 2017, The physical processes of CME/ICME evolution. *Space Sci. Rev.* **212**, 1159.
Mann, G., Klassen, A., Aurass, H., Classen, H.-T.: 2003, Formation and development of shock waves in the solar corona and the near-Sun interplanetary space. *Astron. Astrophys.* **400**, 329.
Mao, S., He, J., Zhang, L., Yang, L., Wang, L.: 2017, Numerical study of erosion, heating, and acceleration of the magnetic cloud as impacted by fast shock. *Astrophys. J.* **842**, 109.
Maricic, D., Vrsnak, B., Dumbovic, M., Zic, T.: 2014, Kinematics of interacting ICMEs and related forbush decrease: case study. *Solar Phys.* **289**, 351. DOI. ADS.
Marubashi, K.: 1986, Structure of the interplanetary magnetic clouds and their solar origins. *Adv. Space Res.* **6**, 335.
Marubashi, K.: 2000, Physics of interplanetary magnetic flux ropes: toward prediction of geomagnetic storms. *Adv. Space Res.* **26**, 55.
Marubashi, K., Akiyama, S., Yashiro, S., Gopalswamy, N., Cho, K.-S., Park, Y.-D.: 2015, Geometrical relationship between interplanetary flux ropes and their solar sources. *Solar Phys.* **290**, 1371. DOI. ADS.
Mays, M.L., Taktakishvili, A., Pulkkinen, A., MacNeice, P.J., Rastaetter, L., Odstrcil, D., *et al.*: 2015, Ensemble modeling of CMEs using the WSA-ENLIL+Cone model. *Solar Phys.* **290**, 1775. DOI. ADS.
Mewaldt, R.A., Looper, M.D., Cohen, C.M.S., Haggerty, D.K., Labrador, A.W., Leske, R.A., Mason, G.M., Mazur, J.E., von Rosenvinge, T.T.: 2012, Energy spectra, composition, and other properties of ground-level events during Solar Cycle 23. *Space Sci. Rev.* **171**, 97.
Mishra, W., Srivastava, N.: 2014, Morphological and kinematic evolution of three interacting coronal mass ejections of 2011 February 13-15. *Astrophys. J.* **794**, 64.
Mishra, W., Wang, Y., Srivastava, N.: 2016, On understanding the nature of collisions of coronal mass ejections observed by STEREO. *Astrophys. J.* **831**, 99.
Morosan, D.E., Carley, E.P., Hayes, L.A., Murray, S.A., Zucca, P., Fallows, R.A., *et al.*: 2019, Multiple regions of shock-accelerated particles during a solar coronal mass ejection. *Nat. Astron.* **3**, 452. DOI.
Möstl, C., Farrugia, C.J., Kilpua, E.K.J., Jian, L.K., Liu, Y., Eastwood, J.P., *et al.*: 2012, Multi-point shock and flux rope analysis of multiple interplanetary coronal mass ejections around 2010 August 1 in the inner heliosphere. *Astrophys. J.* **758**, 10.
Möstl, C., Amla, K., Hall, J.R., Liewer, P.C., De Jong, E.M., Colaninno, R.C., *et al.*: 2014, Connecting speeds, directions and arrival times of 22 coronal mass ejections from the Sun to 1 AU. *Astrophys. J.* **787**, 119.
Möstl, C., Rollett, T., Frahm, R.A., Liu, Y.D., Long, D.M., Colaninno, R.C., Reiss, M.A., Temmer, M., Farrugia, C.J., Posner, A., Dumbović, M., Janvier, M., Démoulin, P., Boakes, P., Devos, A., Kraaikamp, E., Mays, M.L., Vršnak, B.: 2015, Strong coronal channeling and interplanetary evolution of a solar storm up to Earth and Mars. *Nature Comm.* **6**, 7135. DOI.
Möstl, C., Isavnin, A., Boakes, P.D., Kilpua, E.K.J., Davies, J.A., Harrison, R.A., *et al.*: 2017, Modeling observations of solar coronal mass ejections with heliospheric imagers verified with the Heliophysics System Observatory. *Space Weather* **15**, 955. DOI.
Möstl, C., Amerstorfer, T., Palmerio, E., Isavnin, A., Farrugia, C.J., Lowder, C., Winslow, R.M., Donnerer, J.M., Kilpua, E.K.J., Boakes, P.D.: 2018, Forward modeling of coronal mass ejection flux ropes in the inner heliosphere with 3DCORE. *Space Weather* **16**, 216.
Mouschovias, T.C., Poland, A.I.: 1978, Expansion and broadening of coronal loop transients - a theoretical explanation. *Astrophys. J.* **220**, 675.
Müller, D., Zouganelis, I., St. Cyr, O.C., Gilbert, H.R., Nieves-Chinchilla, T.: 2020, Europe's next mission to the Sun. *Nature Astron.* **4**, 205. DOI.
Mulligan, T., Russell, C.T., Luhmann, J.G.: 1998, Solar cycle evolution of the structure of magnetic clouds in the inner heliosphere. *Geophys. Res. Lett.* **25**, 2959.
Nelson, G.J., Melrose, D.B.: 1985, Type II bursts. In: McLean, D.J., Labrum, N.R. (eds.) *Solar Radiophysics: Studies of Emission from the Sun at Metre Wavelengths*, Cambridge University Press, Cambridge, 333.
Niembro, T., Canto, J., Lara, A., Gonzalez, R.F.: 2015, An analytical model of interplanetary coronal mass ejection interactions. *Astrophys. J.* **811**, 2015.
Nieves-Chinchilla, T., Colaninno, R., Vourlidas, A., Szabo, A., Lepping, R.P., Boardsen, S.A., Anderson, B.J., Korth, H.: 2012, Remote and in situ observations of an unusual Earth-directed coronal mass ejection from multiple viewpoints. *J. Geophys. Res.* **117**, 6106.

Nieves-Chinchilla, T., Vourlidas, A., Stenborg, G., Savani, N.P., Koval, A., Szabo, A., Jian, L.K.: 2013, Inner heliospheric evolution of a "stealth" CME derived from multi-view imaging and multipoint in situ observations. I. Propagation to 1 AU. *Astrophys. J.* **779**, 55.

Nieves-Chinchilla, T., Vourlidas, A., Raymond, J.C., Linton, M.G., Al-haddad, N., Savani, N.P., Szabo, A., Hidalgo, M.A.: 2018, Understanding the internal magnetic field configurations of ICMEs using more than 20 years of wind observations. *Solar Phys.* **293**, 25. DOI. ADS.

Nieves-Chinchilla, T., Jian, L.K., Balmaceda, L., Vourlidas, A., dos Santos, L.F.G., Szabo, A.: 2019, Unraveling the internal magnetic field structure of the Earth-directed interplanetary coronal mass ejections during 1995-2015. *Solar Phys.* **294**, 89. DOI.

Odstrcil, D.: 2003, Modeling 3-D solar wind structure. *Adv. Space Res.* **32**, 497.

Odstrcil, D., Pizzo, V.J.: 2009, Numerical heliospheric simulations as assisting tool for interpretation of observations by STEREO heliospheric imagers. *Solar Phys.* **259**, 297. DOI. ADS.

Odstrcil, D., Pizzo, V.J., Arge, C.N.: 2005, Propagation of the 12 May 1997 interplanetary coronal mass ejection in evolving solar wind structures. *J. Geophys. Res.* **110**, 2106.

Odstrcil, D., Savani, N.P., Rouillard, A.P.: 2018, Launching hydrodynamic and magnetic CME-like structures into the operational heliospheric space weather models. In: *Solar Heliospheric and INterplanetary Environment (SHINE) Conf.*, 123. ADS.

Olmedo, O., Gopalswamy, N., Xie, H., Yashiro, S., Makela, P.A., Akiyama, S., St. Cyr, O.C., Vourlidas, A.: 2013, *Forward Fitting of a Coronal Shock Front to a Spheroid*, *Am. Geophys. Union Fall Meet.*, Abstract id. SH13A-2033.

Owens, M.J., Cargill, P.J., Pagel, C., Siscoe, G.L., Crooker, N.U.: 2005, Characteristic magnetic field and speed properties of interplanetary coronal mass ejections and their sheath regions. *J. Geophys. Res.* **110**, 1105.

Palmerio, E., Kilpua, E.K.J., Möstl, C., Bothmer, V., James, A.W., Green, L.M., Isvanin, A., Davies, J.A., Harrison, R.A.: 2018, Coronal magnetic structure of earthbound CMEs and in-situ comparison. *Space Weather* **16**, 442.

Patsourakos, S., Vourlidas, A.: 2012, On the nature and genesis of EUV waves: a synthesis of observations from SOHO, STEREO, SDO and Hinode. *Solar Phys.* **281**, 187. DOI. ADS.

Poedts, S.: 2019, Forecasting space weather with EUHFORIA in the virtual space weather modeling centre. *Plasma Phys. Control. Fusion* **61**, 014011.

Poedts, S., Pomoell, J.P., Zuccarello, F.: 2016, Self-consistent evolution models for slow CMEs up to 1 AU. In: Zhelyazkov, I., Mishonov, T. (eds.) *Black Sea Biennial School and Workshop on Space Plasma Physics* **CP-1714**, AIP, Melville, id. 030002. DOI.

Pomoell, J., Poedts, S.: 2018, EUHFORIA: European heliospheric forecasting information asset. *J. Space Weather Space Clim.* **8**, A35.

Poomvises, W., Zhang, J., Olmedo, O.: 2010, Coronal mass ejection propagation and expansion in three-dimensional space in the heliosphere based on stereo/SECCHI observations. *Astrophys. J. Lett.* **717**, 159.

Prise, A.J., Harra, L.K., Matthews, S.A., Arridge, C.S., Achilleos, N.: 2015, Analysis of a coronal mass ejection and corotating interaction region as they travel from the Sun passing Venus, Earth, Mars, and Saturn. *J. Geophys. Res.* **120**, 1566.

Qiu, J., Yurchyshyn, V.B.: 2005, Magnetic reconnection flux and coronal mass ejection velocity. *Astrophys. J. Lett.* **634**, L121.

Qiu, J., Hu, Q., Howard, T.A., Yurchyshyn, V.B.: 2007, On the magnetic flux budget in low-corona magnetic reconnection and interplanetary coronal mass ejections. *Astrophys. J.* **659**, 758.

Reames, D.V.: 2009, Solar energetic-particle release times in historic ground-level events. *Astrophys. J.* **706**, 844.

Reames, D.V.: 2017, *Energetic Particles*, Springer, Berlin. DOI.

Reiff, P.H., Daou, A.G., Sazykin, S.Y., Nakamura, R., Hairston, M.R., Coffey, V., *et al.*: 2016, Multispacecraft observations and modeling of the 22/23 June 2015 geomagnetic storm. *Geophys. Res. Lett.* **43**, 7311.

Reinard, A.A.: 2008, Analysis of interplanetary coronal mass ejection parameters as a function of energetics, source location, and magnetic structure. *Astrophys. J.* **682**, 1289.

Reinard, A.A., Lynch, B.J., Mulligan, T.: 2012, Composition structure of interplanetary coronal mass ejections from multispacecraft observations, modeling, and comparison with numerical simulations. *Astrophys. J.* **761**, 175.

Richardson, I.G., Cane, H.V.: 2004, The fraction of interplanetary coronal mass ejections that are magnetic clouds: evidence for a solar cycle variation. *Geophys. Res. Lett.* **31**, L18804. DOI.

Riley, P., Linker, J.A., Lionello, R., Mikić, Z., Odstrcil, D., Hidalgo, M.A., Cid, C., Hu, Q., Lepping, R.P., Lynch, B.J., Rees, A.: 2004, Fitting flux ropes to a global MHD solution: a comparison of techniques. *J. Atmos. Solar-Terr. Phys.* **66**, 1321. DOI.

Riley, P., Mays, L., Andries, J., Amerstorfer, T., Biesecker, D., Delouille, V., *et al.*: 2018, Forecasting the arrival time of coronal mass ejections: analysis of the CCMC CME scoreboard. *Space Weather* **16**, 1245.
Rouillard, A.P.: 2011, Relating white light and in situ observations of coronal mass ejections: a review. *J. Atmos. Solar-Terr. Phys.* **73**, 1201.
Rouillard, A.P., Odstrcil, D., Sheeley, N.R., Tylka, A., Vourlidas, A., Mason, G., *et al.*: 2011, Interpreting the properties of solar energetic particle events by using combined imaging and modeling of interplanetary shocks. *Astrophys. J.* **735**, 7.
Ruffenach, A., Lavraud, B., Owens, M.J., Sauvaud, J.A., Savani, N.P., Rouillard, A.P., *et al.*: 2012, Multispacecraft observation of magnetic cloud erosion by magnetic reconnection during propagation. *J. Geophys. Res.* **117**, 9101.
Ruffenach, A., Lavraud, B., Farrugia, C.J., Démoulin, P., Dasso, S., Owens, M.J., *et al.*: 2015, Statistical study of magnetic cloud erosion by magnetic reconnection. *J. Geophys. Res.* **120**, 43.
Russell, C.T.: 2000, The solar wind interaction with the Earth's magnetosphere: a tutorial. *IEEE Trans. Plasma Sci.* **28**, 1818.
Russell, C.T., Mewaldt, R.A., Luhmann, J.G., Mason, G.M., von Rosenvinge, T.T., Cohen, C.M.S., *et al.*: 2013, The very unusual interplanetary coronal mass ejection of 2012 July 23: a blast wave mediated by solar energetic particles. *Astrophys. J.* **770**, 38.
Savani, N.P., Rouillard, A.P., Davies, J.A., Owens, M.J., Forsyth, R.J., Davis, C.J., Harrison, R.A.: 2009, The radial width of a coronal mass ejection between 0.1 and 0.4 AU estimated from the heliospheric imager on STEREO. *Ann. Geophys.* **27**, 4349.
Savani, N.P., Owens, M.J., Rouillard, A.P., Forsyth, R.J., Davies, J.A.: 2010, Observational evidence of a coronal mass ejection distortion directly attributable to a structured solar wind. *Astrophys. J. Lett.* **714**, L128.
Savani, N.P., Owens, M.J., Rouillard, A.P., Forsyth, R.J., Kusano, K., Shiota, D., Kataoka, R.: 2011a, Evolution of coronal mass ejection morphology with increasing heliocentric distance. I. Geometrical analysis. *Astrophys. J.* **731**, 109.
Savani, N.P., Owens, M.J., Rouillard, A.P., Forsyth, R.J., Kusano, K., Shiota, D., Kataoka, R., Jian, L., Bothmer, V.: 2011b, Evolution of coronal mass ejection morphology with increasing heliocentric distance. II. In situ observations. *Astrophys. J.* **732**, 117.
Savani, N.P., Davies, J.A., Davis, C.J., Shiota, D., Rouillard, A.P.: 2012, Observational tracking of the 2D structure of coronal mass ejections between the Sun and 1 AU. *Solar Phys.* **279**, 517. DOI. ADS.
Savani, N.P., Vourlidas, A., Shiota, D., Linton, M.G., Kusano, K., Lugaz, N., Rouillard, A.P.: 2013, A plasma ß transition within a propagating flux rope. *Astrophys. J.* **779**, 142.
Savani, N.P., Vourlidas, A., Szabo, A., Mays, M.L., Richardson, I.G., Thompson, B.J., Pulkkinen, A., Evans, R., Nieves-Chinchilla, T.: 2015, Predicting the magnetic vectors within coronal mass ejections arriving at Earth: 1. Initial architecture. *Space Weather* **13**, 374.
Schmidt, J.M., Cargill, P.J.: 2004, A numerical study of two interacting coronal mass ejections. *Ann. Geophys.* **22**, 2245.
Scolini, C., Rodriguez, L., Mierla, M., Pomoell, J., Poedts, S.: 2019, Observation-based modelling of magnetised coronal mass ejections with EUHFORIA. *Astron. Astrophys.* **626**, A122. DOI.
Shen, C., Wang, Y., Wang, S., Liu, Y.D., Liu, R., Vourlidas, A., Miao, B., Ye, P., Liu, J., Zhou, Z.: 2012, Super-elastic collision of large-scale magnetized plasmoids in the heliosphere. *Nat. Phys.* **8**, 923.
Shen, F., Shen, C., Wang, Y., Feng, X., Xiang, C.: 2013, Could the collision of CMEs in the heliosphere be superelastic? Validation through three-dimensional simulations. *Geophys. Res. Lett.* **40**, 1457. DOI.
Shen, C., Wang, Y., Pan, C., Miao, B., Ye, P., Wang, S.: 2014, Full-halo coronal mass ejections: arrival at the Earth. *J. Geophys. Res.* **119**, 5107.
Shen, C., Xu, M., Wang, Y., Chi, Y., Luo, B.: 2018, Why the shock-ICME complex structure is important: learning from the early 2017 September CMEs. *Astrophys. J.* **861**, 28. DOI.
Shiota, D., Kataoka, R.: 2016, Magnetohydrodynamic simulation of interplanetary propagation of multiple coronal mass ejections with internal magnetic flux rope (SUSANOO-CME). *Space Weather* **14**, 56.
Singh, T., Yalim, M.S., Pogorelov, N.V., Gopalswamy, N.: 2019, Simulating solar coronal mass ejections constrained by observations of their speed and poloidal flux. *Astrophys. J. Lett.* **875**, L17.
Siscoe, G., Odstrcil, D.: 2008, Ways in which ICME sheaths differ from magnetosheaths. *J. Geophys. Res.* **113**, A00B07.
Sterling, A.C.: 2018, Coronal jets and the jet-CME connection. In: Zank, G.P. (ed.) *Proc. 17th Ann. Int. Astrophys. Conf., J. Phys.* **CS-1100**, IOP, Bristol, 012024. DOI.
Temmer, M., Nitta, N.: 2015, Interplanetary propagation behavior of the fast coronal mass ejection on 23 July 2012. *Solar Phys.* **290**, 919. DOI. ADS.
Temmer, M., Vrsnak, B., Rollett, T., Bein, B., de Koning, C., Liu, Y., Bosman, E., Davies, J.A., Möstl, C., Zic, T.: 2012, Characteristics of kinematics of a coronal mass ejection during the 2010 August 1 CME-CME interaction event. *Astrophys. J.* **749**, 57.

Temmer, M., Veronig, A.M., Peinhart, V., Vrsnak, B.: 2014, Asymmetry in the CME-CME interaction process for the events from 2011 February 14-15. *Astrophys. J.* **785**, 85.

Thakur, N., Gopalswamy, N., Xie, H., Mäkelä, P., Yashiro, S., Akiyama, S., Davila, J.M.: 2014, Ground level enhancement in the 2014 January 6 solar energetic particle event. *Astrophys. J. Lett.* **790**, L13.

Thernisien, A.: 2011, Implementation of the graduated cylindrical shell model for the three-dimensional reconstruction of coronal mass ejections. *Astrophys. J. Suppl.* **194**, 33.

Thernisien, A., Vourlidas, A., Howard, R.A.: 2009, Forward modeling of coronal mass ejections using STEREO/SECCHI data. *Solar Phys.* **256**, 111. DOI. ADS.

Török, T., Panasenco, O., Titov, V.S., Mikič, Z., Reeves, K.K., Velli, M., Linker, J.A., de Toma, G.: 2011, A model for magnetically coupled sympathetic eruptions. *Astrophys. J. Lett.* **739**, L63.

Török, T., Downs, C., Linker, J.A., Lionello, R., Titov, V.S., Mikič, Z., Riley, P., Caplan, R.M., Wijaya, J.: 2018, Sun-to-Earth MHD simulation of the 2000 July 14 "Bastille Day" eruption. *Astrophys. J.* **856**, 75.

Vandas, M.S., Fischer, P., Pelant, M., Dryer, M., Smith, Z., Detman, T.: 1997, Propagation of a spheromak: 1. Some comparisons of cylindrical and spherical magnetic clouds. *J. Geophys. Res.* **2012**, 24183.

Verbeke, C., Pomoell, J., Poedts, S.: 2019, The evolution of coronal mass ejections in the inner heliosphere: implementing the spheromak model with EUHFORIA. *Astron. Astrophys.* **627**, A111. DOI.

Veronig, A.M., Muhr, N., Kienreich, I.W., Temmer, M., Vršnak, B.: 2010, First observations of a dome-shaped large-scale coronal extreme-ultraviolet wave. *Astrophys. J. Lett.* **716**, L57.

Vourlidas, A., Webb, D.F.: 2018, Streamer-blowout coronal mass ejections: their properties and relation to the coronal magnetic field structure. *Astrophys. J.* **861**, 103.

Vourlidas, A., Lynch, B.J., Howard, R.A., Li, Y.: 2013, How many CMEs have flux ropes? Deciphering the signatures of shocks, flux ropes, and prominences in coronagraph observations of CMEs. *Solar Phys.* **284**, 179. DOI. ADS.

Vourlidas, A., Balmaceda, L.A., Stenborg, G., Dal Lago, A.: 2017, Multi-viewpoint coronal mass ejection catalog based on STEREO COR2 observations. *Astrophys. J.* **838**, 17. DOI. ADS.

Vršnak, B., Žic, T., Vrbanec, D., Temmer, M., Rollett, T., Möstl, C., *et al.*: 2013, Propagation of interplanetary coronal mass ejections: the drag-based model. *Solar Phys.* **285**, 295. DOI. ADS.

Vršnak, B., Temmer, M., Žic, T., Taktakishvili, A., Dumbovic, M., Möstl, C., Veronig, A.M., Mays, M.L., Odstrcil, D.: 2014, Heliospheric propagation of coronal mass ejections: comparison of numerical WSA-ENLIL+Cone model and analytical drag-based model. *Astrophys. J. Suppl.* **213**, 21.

Wang, Y., Wang, B., Shen, C., Shen, F., Lugaz, N.: 2014, Deflected propagation of a coronal mass ejection from the corona to interplanetary space. *J. Geophys. Res.* **119**, 5117.

Webb, D.F., Howard, T.A.: 2012, Coronal mass ejections: observations. *Liv. Rev. Solar Phys.* **9**, 3.

Webb, D.F., Möstl, C., Jackson, B.V., Bisi, M.M., Howard, T.A., Mulligan, T., *et al.*: 2013, Heliospheric imaging of 3D density structures during the multiple coronal mass ejections of late July to early August 2010. *Solar Phys.* **285**, 317. DOI. ADS.

Wilson, R.M.: 1987, Geomagnetic response to magnetic clouds. *Planet. Space Sci.* **35**, 329.

Winslow, R.M., Lugaz, N., Philpott, L.C., Schwadron, N.A., Farrugia, C.J., Anderson, B.J., Smith, C.W.: 2015, Interplanetary coronal mass ejections from MESSENGER orbital observations at Mercury. *J. Geophys. Res.* **120**, 6101. DOI.

Winslow, R.M., Lugaz, N., Schwadron, N.A., Farrugia, C.J., Yu, W., Raines, J.M., Mays, M.L., Galvin, A.B., Zurbuchen, T.H.: 2016, Longitudinal conjunction between MESSENGER and STEREO a: development of ICME complexity through stream interactions. *J. Geophys. Res.* **121**, 6092.

Witasse, O., Sánchez-Cano, B., Mays, M.L., Kajdič, P., Opgenoorth, H., Elliott, H.A., *et al.*: 2017, Interplanetary coronal mass ejection observed at STEREO-A, Mars, Comet 67P/Churyumov-Gerasimenko, Saturn, and New Horizons en route to Pluto: comparison of its forbush decreases at 1.4, 3.1, and 9.9 AU. *J. Geophys. Res.* **122**, 7865.

Wold, A.M., Mays, M.L., Taktakishvili, A., Jian, L.K., Odstrcil, D., MacNeice, P.: 2018, Verification of real-time WSA-ENLIL+Cone simulations of CME arrival-time at the CCMC from 2010 to 2016. *J. Space Weather Space Clim.* **8**, A17.

Wood, B.E., Howard, R.: 2009, An empirical reconstruction of the 2008 April 26 coronal mass ejection. *Astrophys. J.* **702**, 901.

Wood, B.E., Wu, C.-C., Howard, R.A., Socker, D.G., Rouillard, A.P.: 2011, Empirical reconstruction and numerical modeling of the first geoeffective coronal mass ejection of Solar Cycle 24. *Astrophys. J.* **729**, 70.

Wood, B.E., Wu, C.-C., Rouillard, A.P., Howard, R.A., Socker, D.G.: 2012, A coronal hole's effects on coronal mass ejection shock morphology in the inner heliosphere. *Astrophys. J.* **755**, 43.

Wood, B.E., Wu, C.-C., Lepping, R.P., Nieves-Chinchilla, T., Howard, R.A., Linton, M.G., Socker, D.G.: 2017, A STEREO survey of magnetic cloud coronal mass ejections observed at Earth in 2008-2012. *Astrophys. J.* **229**, 29.

Xie, H., Gopalswamy, N., St. Cyr, O.C.: 2013, Near-sun flux-rope structure of CMEs. *Solar Phys.* **284**, 47. DOI. ADS.

Xie, H., Ofman, L., Lawrence, G.: 2004, Cone model for halo CMEs: application to space weather forecasting. *J. Geophys. Res.* **109**, 3109.

Xie, H., Gopalswamy, N., Ofman, L., St. Cyr, O.C., Michalek, G., Lara, A., Yashiro, S.: 2006, Improved input to the empirical coronal mass ejection (CME) driven shock arrival model from CME cone models. *Space Weather* **4**, S10002.

Xie, H., Mäkelä, P., St. Cyr, O.C., Gopalswamy, N.: 2017, Comparison of the coronal mass ejection shock acceleration of three widespread SEP events during solar cycle 24. *J. Geophys. Res.* **122**, 7021.

Yashiro, S., Gopalswamy, N., Mäkelä, P., Akiyama, S.: 2013, Post eruption arcades and interplanetary coronal mass ejections. *Solar Phys.* **284**, 5. DOI. ADS.

Yurchyshyn, V., Abramenko, V., Tripathi, D.: 2009, Rotation of white-light coronal mass ejection structures as inferred from LASCO coronagraph. *Astrophys. J.* **705**, 426.

Zucca, P., Morosan, D.E., Rouillard, A.P., Fallows, R., Gallagher, P.T., Magdalenic, J., *et al.*: 2018, Shock location and CME 3D reconstruction of a solar type II radio burst with LOFAR. *Astron. Astrophys.* **615**, A89. DOI.

Zurbuchen, T.H., Richardson, I.G.: 2006, In-situ solar wind and magnetic field signatures on interplanetary coronal mass ejections. *Space Sci. Rev.* **123**, 31. DOI.